Targeted Delivery to the Central Nervous System utilizing Magnetically Guided Immunomagnetoliposomes

Master' s Thesis in Medicine with industrial Specialization, June 2012

by
Thomas Linemann

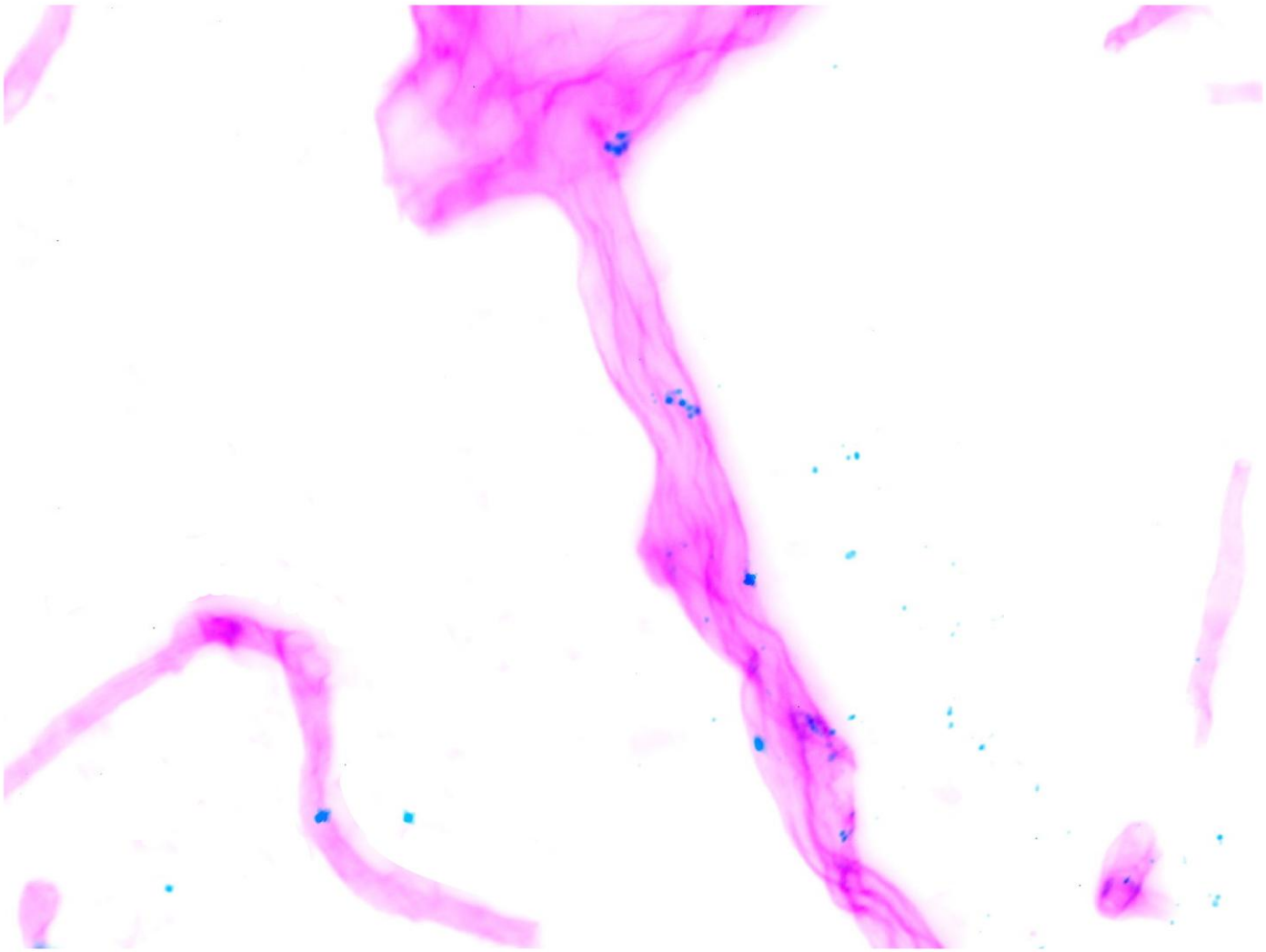

AALBORG UNIVERSITY

Department of Health Science and Technology
Laboratory of Neurobiology

Preface

This Master's thesis represents the conclusion of my Master Program in Medicine with Industrial Specialization at the Department of Health Science and Technology, Aalborg University. The experimental work of this thesis was carried out at the Laboratory of Neurobiology in the period of September 2011 to June 2012.

I wish to thank laboratory technician Merete Fredsgaard for always being helpful and providing competent advice.

I also want to extent my gratitude to Professor, dr.med, Ph.D Svend Birkelund for assisting and providing expertise on hybridoma cell culture and antibody purification.

I am grateful to Assistant Professor, Ph.D. Louiza Bohn Thomsen for reading and commenting on the Master's thesis manuscript.

Furthermore I would like to thank Novo Nordisk A/S for financial support.

Finally I would like to thank my supervisor Professor, dr.med, Ph.D. Torben Moos for great support and encouragement.

The thesis is structured as a scientific article and the referencing is done according to the Harvard-method.

Title: Targeted Delivery to the Central Nervous System utilizing Magnetically Guided Immunomagnetoliposomes

Numbers printed: 4

Number of pages: 42

Appendix: 1

Finished: 1st of June 2012

_____

Thomas Linemann, 1st of June 2012

Abstract

Background: The delivery of therapeutics across the blood-brain barrier (BBB) constitutes a significant hurdle for the treatment of patients suffering from CNS disorders. This is especially evident for neurodegenerative diseases such as Alzheimer's and Parkinson's disease, since the BBB limits the treatment options to small lipophilic drugs, which has a limited therapeutic potential. Therefore several nanoparticulate drug delivery systems are being investigated to enable macromolecular drug delivery to the CNS and thereby improving the treatment options.

Methods: The purpose of this study was to construct a magnetic responsive drug delivery system to enable drug delivery across the BBB. The starting platform was starch coated magnetic nanoparticles (S-MNPs), which were encapsulated in phospholipids to yield magnetoliposomes (MLs). Finally OX26 antibodies, targeting the transferrin receptor, was purified from an in-house hybridoma cell culture and utilized to produce OX26 conjugated magnetoliposomes (OX26-MLs). Initially cellular uptake of all particle types were screened in vitro in rat brain endothelial cells (RBE4 cells). The biodistribution of MLs and OX26-MLs was investigated after intravenous injection in 16 day old rats (P16). The morphological biodistribution was studied on tissue sections from brain, liver, spleen, lungs, and kidneys by fluorescence microscopy. Finally the ability of MLs and OX26-MLs to traverse the BBB both with and without the application of a magnetic field was tested on P16 rats using the in situ brain perfusion method (n = 10). Traversal of the BBB was evaluated by immunohistochemical staining of laminin in the basement membrane of the capillary bed, and sections were then analyzed by fluorescence microscopy to detect particles beyond the BBB. P16 rats were used due to their high expression and recycling rate of transferrin receptors in the brain capillary endothelial cells (BCECs).

Results: In vitro screening of the cellular uptake in RBE4 cells revealed a 4.3 fold and 7.3 fold increase in median cell fluorescence intensity for MLs and OX26-MLs compared to S-MNPs, respectively. Furthermore OX26-MLs demonstrated a 1.6 fold increase compared to MLs. Mann-Whitney-U tests revealed that all groups were significantly different from each other ($p < 0.05$). The biodistribution revealed a preferential uptake of both MLs and OX26-MLs in the liver and spleen, whereas a small amount of particles were present in the lungs and virtually absent in the kidney. Surprisingly no significant accumulation of both MLs and OX26-MLs were seen in the brain capillaries. In situ brain perfusion experiments revealed, that OX26-MLs demonstrated a good potential as a drug delivery system to the BCECs with enhanced uptake compared to MLs. Furthermore the uptake did not dependent on an external magnetic field and hence OX26-MLs are probably transported into the BCECs by receptor mediated endocytosis. When investigating the permeation of OX26-MLs under the influence of a magnetic field a small amount of OX26-MLs was found beyond the BBB, which suggests transcytosis occurred. However, no convincing and consistent evidence was found for this phenomenon to support widespread transcytosis and cellular accumulation of OX26-MLs beyond the BBB.

Conclusion: OX26-MLs were synthesized and constitute a novel drug delivery system, which has the ability to target the BCECs. This suggests that OX26-MLs are suitable for blood to endothelium transport. However, the potential of OX26-MLs to enhance the permeation of the BBB remains obscure. Furthermore the stability in blood must be improved to make intravenous administration feasible.

Abbreviations: AMT Adsorptive-mediated transport · **AUC** Area under the time concentration curve · **BBB** Blood-Brain Barrier · **BCECs** Brain Capillary Endothelial Cells · **BDNF** brian-derived neurotrophic factor · **CNS** Central Nervous System · **CSF** · Cerebrospinal fluid **DDAB** · Dimethyldioctadecylammonium bromide · **DMT-1** Divalent metal transporter-1 · **DSPE-PEG2000-MAL** 1,2-distearoyl-sn-glycero-3-phosphoethanolamine-N-[maleimide(polye-thylene glycol)-2000] · **GDNF** glial-derived neurotrophic factor · **IHC** Immunohistochemistry · **i.v.** Intravenous · **mPEG2000-PE** 1,2-dipalmitoyl-sn-glycero-3-phosphoethanolamine-N-methoxy(polyethylene glycol)-2000 · **MLs** Magnetoliposomes · **MNPs** · Magnetic nanoparticles · **MRI** Magnetic resonance imaging · **OX26-MLs** OX26 conjugated magnetoliposomes · **P16 rats** 16 days old rats · **VIPa** vasoactive intestinal peptide analog · **PDI** Polydispersity index · **PEG** Polyethylene glycol · **PILs** · PEGylated immunoliposomes · **RBE4** Rat brain endothelial Cells · **RES** Reticuloendothelial system · **RMT** Receptor-mediated transcytosis · **SDS** sodium dodecyl sulfate · **S-MNPs** Starch-coated magnetic nanoparticles · **SOY PC** L-α-phosphatidylcholine · **SD rats** Sprague Dawley · **TH** tyrosine hydroxylase · **ZO** Zona Occludens

Table of Content

1. Introduction

Development of effective therapeutics for patients suffering from disorders affecting the central nervous system (CNS) has long been halted due to the blood-brain barrier (BBB) [Pardridge, 2005]. CNS disorders such as Alzheimer's disease are threatening to break the healthcare system by huge increases in treatment and care costs [Mount & Downton, 2006]. In Denmark dementia is estimated to cost 9.5 to 15 billion Danish kroner with Alzheimer's disease contributing with 75% of the total cost while the worldwide cost of Alzheimer's disease is estimated to be 1% of the World's gross domestic product [Nationalt Videnscenter for Demens, 2011; Nationalt Videnscenter for Demens, 2012]. Although huge efforts are put into the development of new therapeutics, this might be a flawed approach as the actual hurdle is not the lack of therapeutics, but the fact that effective therapeutics are impossible to deliver efficiently to the CNS [Pardridge, 2010].

The BBB is formed by the brain capillary endothelial cells (BCECs), which are held closely together by tight junctions and thereby restricts the transport of therapeutics by the paracellular route [Abbott *et al.*, 2010]. Thus, only therapeutics which are highly lipophilic or which can utilize the natural occurring transport mechanisms on the BCECs, can gain access to the brain parenchyma. Developing drug delivery systems targeting endogenous receptors of the brain are now considered the most promising approach to transport therapeutics into the brain [Gabathuler, 2010]. The target for such drug delivery systems could be the transferrin receptor, insulin receptor or the melanotransferrin receptor expressed by the BCECs, which upon binding to their respective ligands undergo endocytosis [Gabathuler, 2010] .

Magnetoliposomes (MLs) are a fairly unexplored drug delivery system. This hybrid delivery system benefits from both liposome technology and the magnetic susceptibility of magnetic nanoparticle technology, which enables magnetic guidance of the particles by an external magnet. The liposome shields the magnetic nanoparticle in a lipid bilayer, which can contain polyethylene glycol conjugated phospholipids (PEGylated phospholipids) in order to increase the plasma half-life. In addition the PEGylated phospholipids can be functionalized by conjugating targeting ligands to the distal end of the PEG polymer [Allen, 1994; Martina *et al.*, 2005].

Conjugating anti-transferrin receptor antibodies to drug delivery systems has been investigated to direct blood to brain delivery of therapeutics. The monoclonal antibody OX26 targets the transferrin receptor and is employed in rats due to the fact, that BCECs display a high expression of transferrin receptors, which are not expressed by endothelia in the rest of the body [Jefferies *et al.*, 1984]. The transferrin receptor is internalized upon binding to OX26; however, the subsequent events are substance for much controversy. While some researchers claim that transcytosis occurs followed by release of the complex to the brain parenchyma [Friden *et al.*, 1991; Huwyler *et al.*, 1997] others argue that the transferrin receptor is recycled back to the luminal side [Roberts *et al.*, 1993; Moos & Morgan, 2001]. However all investigators agree that OX26 targeted delivery systems will accumulate in the BCECs at first. Our research group has never encountered convincing evidence to support the notion, that OX26 targeted delivery systems are transcytosed through the BCECs and enter the parenchyma. Hence, another method must be employed in order to facilitate endothelium to brain transport. The use of an external magnetic field may prove to be a feasible method, to facilitate the movement of magnetic nanoparticles trapped inside the BCECs and direct them to the brain parenchyma enabling endothelium to brain transport. Our research group have previously exploited this in a Transwell-system, an in vitro BBB model, and demonstrated that an external magnet can facilitate the release of particles accumulated in the BCECs (unpublished).

Thus, the aim of the thesis at hand was to develop a magnetic responsive drug delivery system, which would be able to target the BCECs by using OX26 as a targeting ligand and exit the BCECs again facilitated by an external magnet.

MLs and OX26 conjugated MLs (OX26-MLs) were synthesized and their capability to cross the BBB under the influence of an external magnetic field was evaluated using the in situ brain perfusion technique in 16 days old Wistar rats. The benefit of using 16 days old rats (P16 rats) is the fact that their BCECs express the transferrin receptor to a much higher degree than adult rats [Moos & Morgan, 2001]. Furthermore, the morphological biodistribution of OX26-MLs was compared to unconjugated MLs in the brain, spleen, liver, lungs and the kidneys.

1.1 The Blood-Brain Barrier

Homeostasis in the microenvironment of the brain parenchyma is a necessity for normal neuronal functioning and signalling. Neurons are extremely fragile cells with the need for a constant supply of oxygen and nutrients, precise regulation of ions and neurotransmitters and protection from toxic compounds and pathogens, which must therefore be excluded from the CNS parenchyma [Wolburg & Lippoldt, 2002]. These homeostatic tasks are carried out almost exclusively by a tightly regulated vascular-unit located at the interface between the blood and CNS composed primarily of the BCECs, which interacts with pericytes, astrocytes, neurons and the basement membrane [Cardoso *et al.*, 2010]. Together this cellular unit compose the BBB (Figure 2). Transport across the BBB is strictly controlled by the presence of tight junctions between the BCECs but also due to metabolic enzymes and a diversity of transport systems present in the BCECs [Abbott *et al.*, 2010].

Although other barrier systems exist within the CNS in addition to the BBB, namely the arachnoid epithelial membrane covering the surface of the brain and spinal cord and the blood-cerebrospinal-fluid (CSF) barrier located at the epithelium of choroid plexus, none of these barriers are quantitatively important barrier systems, as the surface area of the BBB are more than 1000-fold greater than the surface area of either the blood-CSF barrier or the arachnoid epithelial membrane in the human brain [Dohrmann, 1970; Pardridge, 2002]. Therefore, when considering barrier systems in the brain the main focus is the BBB composed of more than 600 km of capillaries with an overall surface area of approximately 20 m^2 in the human brain [Pardridge, 2003].

1.1.1 Structural Components of the Blood-Brain Barrier

The anatomic basis of the BBB is provided by a continuous capillary network, which is formed by BCECs situated at the interface between the blood and the brain parenchyma. The BCECs are linked together by junctional complexes and regulate transport of micro- and macromolecules, leukocyte trafficking and osmoregulation [Persidsky *et al.*, 2006]. In addition BCECs have a key role in neurogenesis by secretion of several growth factors and providing neurogenic niches [Cardoso *et al.*, 2010]. The structural components of the BCECs responsible for reducing the paracellular transportation to a minimum are the junctions between the cells, namely adherens junctions and tight junctions (Figure 1) [Wolburg *et al.*, 2009; Abbott *et al.*, 2010]. The adherens junctions are situated in basolateral part of the BCECs and provide tight cell to cell contact, which stabilizes the vascular structure [Wolburg *et al.*, 2009]. The adherens junctions are composed of cadherin proteins, which span the intercellular cleft and connect to the cytoskeleton through intracellular catenin proteins. In addition to their structural function adherens junctions have a regulatory role in tight junction formation and thereby disruption of adherens junction will compromise the BBB integrity [Wolburg & Lippoldt, 2002].

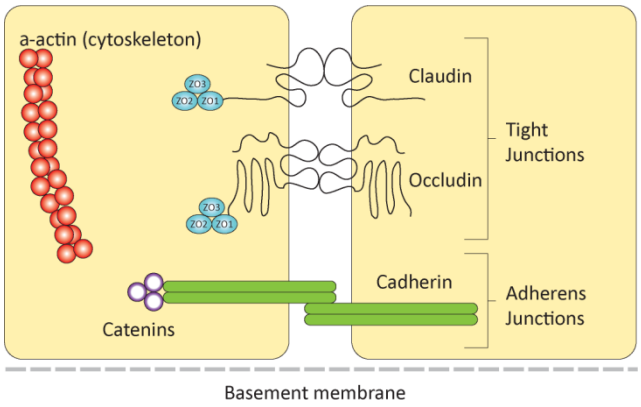

Figure 1: Illustrates two BCECs and their connections through tight and adherens junctions. The adherens junction consists of cadherin, which spans intercellular cleft and interacts with the cytoskeleton through contact with intracellular catenin proteins. The tight-junctions are composed of two major proteins, occludin and claudins, which interact with claudins and occludin, respectively. Occludin and claudins are connected to the regulatory proteins ZO-1, ZO-2 and ZO-3 in the cytosol of the BCECs, which are involved in the regulation of the BBB integrity. Together the adherens junction and tight junctions are responsible for restricting paracellular transport across the BBB.

Modified from [Abbott et al., 2010]

The tight junctions consist of three major protein types, which include junctional adhesion molecules, occludin, and claudins. Both occludin and claudins span the intercellular cleft and thereby mediate cell-to-cell contact. Claudins seem to fulfil the task of establishing the paracellular barrier properties, whereas occludin acts more as an additional supportive structure to further increase the tightness [Wolburg & Lippoldt, 2002; Persidsky *et al.*, 2006]. Both protein types are linked to intracellular regulatory proteins called zonula occludens-1 (ZO-1), ZO-2, ZO-3, which interact with the cytoskeleton through cingulin (Figure 1) [Wolburg & Lippoldt, 2002]. Although tight

junctions are responsible for the barrier properties of the BBB the junctions should not be considered static, as changes in the brain microenvironment can alter the tight junction properties, and thereby the BBB permeability [Wolburg *et al.*, 2009]. The last class of junctional proteins are the junctional adhesion molecules; however, these are not involved in the barrier properties but are highly involved in leukocyte diapedesis, which is especially important in inflammatory diseases [Zlokovic, 2008].

The main function of the tight junctions is to restrict paracellular transport of ions, polar solutes, and macromolecules. The relative impermeability to polar solutes and ions results in a high transendothelial electrical resistance across the BBB of approximately 1800 Ω/cm 2 in rats [Butt et al., 1990]. This high electrical resistance highlights the low conductance of the paracellular pathway and emphasizes the extreme effectiveness of the tight junctions to restrict the movement of polar solutes across the BBB [Abbott *et al.*, 2010].

Although the BCECs and their connections through tight junctions and the adherens junctions are important for the barrier properties, other components also contribute to the barrier by supporting the BCECs both through direct contact but also through soluble factors, which serves to maintain the barrier functions (Figure 2). The basement membrane consists of a meshwork of extracellular proteins including collagen, elastin, fibronectin and laminin as well as some proteoglycans [Cardoso *et al.*, 2010]. The basement membrane surrounds the BCECs and is responsible for anchoring the BCECs in place and establishing their connection with the brain parenchyma. Disruption of the basement membrane leads to alterations in the interactions with the cytoskeleton of the BCECs, which may alter the tight junctions' integrity. In addition the basement membrane can probably serve as a physiological barrier distal to the BBB by tapping and limiting passage of molecules, which have passed the BCECs [Muldoon *et al.*, 1999]. The basement membrane furthermore imbeds another important cell type located at the BBB interface, namely the pericyte [Cardoso *et al.*, 2010].

The pericyte is imbedded in the basement membrane, but sends out projections that interact with the BCECs and covers 22-32 % of the circumference of the brain capillaries [Kim *et al.*, 2005]. Pericytes have a rich content of α-smooth muscle actin, which suggest a contractile nature of these cells. The ability to contract has been demonstrated in vitro as well as in vivo where pericytes are regulating the blood flow through capillaries of the brain [Kelley *et al.*, 1987; Peppiatt *et al.*, 2006]. The pericytes both physically communicate with BCECs through gap-junctions and tight-junctions but also through soluble factors [Allt & Lawrenson, 2001; Bagley *et al.*, 2005]. The intimate connection between pericytes and BCECs reflects the pericytes role in proliferation, migration and differentiation of the BCECs and consequently their absence leads to an abnormal vascular morphology and hyperplasia.

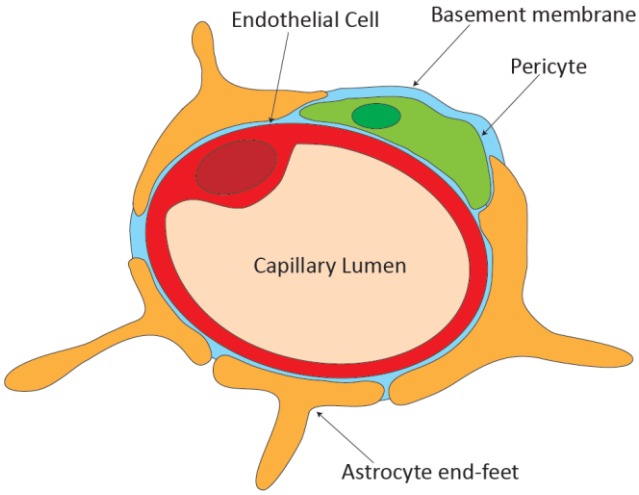

Figure 2: Depicts the structural composition and interactions at the BBB. The BCECs rest on a basement membrane, which imbeds the pericytes. The pericytes send out projections, which partially covers the circumference of capillary. In addition astrocytes are seen with their end-feet processes, which nearly envelope the entire capillary.

Modified from [Abbott et al., 2010]

Astrocytes contribute to the BBB interface by establishing contact with more than 99% of the basal membrane. This is achieved by the end-feet of the astrocytes, which form a lace of fine lamellae resting on the basement membrane [Abbott, 2002]. Although astrocytes are not in direct contact with the BCECs, they synthesis soluble factors, which are very important for the induction and maintenance of the barrier-properties of the BBB [Abbott, 2002].

The restrictive nature of the BBB isolates the brain from many essential nutrients, hormones and proteins, and as a response a diverse range of transport mechanisms reside in the BCECs in order to supply the brain parenchyma with essential substances. These transport mechanisms include solute carriers, receptor- and adsorptive mediated transcytosis. Finally efflux-transporters are also present in

the BCECs, and these transporters are important for protecting the brain against harmful substances.

1.2 Transport across the Blood-Brain Barrier

1.2.1 Solute Carriers

The barrier formed by tight junctions effectively restricts paracellular diffusion to such a degree that essential polar nutrients such as glucose and amino acids are completely restricted from the brain parenchyma. Therefore the BBB must contain a range of specific solute carriers for these vital nutrients necessary for normal brain metabolism and function [Abbott *et al.*, 2010]. Some of these solute carriers display a polarized expression at either the luminal or abluminal membrane of the BCECs, whereas others are expressed evenly between both membranes. As a result of the orientation of these transporters the transport of substances can preferentially be directed into or across the BCECs and the direction may be favoured from the blood to the brain or brain to blood [Abbott *et al.*, 2010]. An example of a solute carrier is the glucose transporter-1, which is expressed both luminal and abluminal and is therefore bi-directional and intended to ensure homeostatic control of the glucose concentration in the brain parenchyma by avoiding accumulation of glucose at higher levels than plasma [Zlokovic, 2008].

1.2.2 Efflux Transporters

The ATP-binding cassette family contains a number of efflux-transporters (ABC-transporters), which are membrane bound and utilize ATP to pump drugs, drug metabolites and endogenous metabolites out of cells [Dallas *et al.*, 2006]. A wide range of ABC-transporters are present in the BCECs and actively transport a diverse range of solutes out of the BCECs and the CNS. The role of ABC-transporters is neuroprotection by removal of potentially neurotoxic endogenous or xenobiotic molecules, but unfortunately also a wide range of therapeutics are substrates for these transporters [Dallas *et al.*, 2006]. ABC-transporters provide an explanation for the lower entry rate of many lipophilic drugs and solutes to the CNS parenchyma, than would be expected from their partition coefficients [Abbott *et al.*, 2010]. The most important ABC-transporters in the BCECs, are the P-glycoprotein, the multidrug resistance-associated proteins, and the breast cancer resistance protein [Abbott *et al.*, 2010]. Recent studies have demonstrated increased density of both the P-glycoprotein and the breast cancer resistance protein on the luminal compared to the abluminal membrane of the BCECs. This suggests that substrates of the ABC-transporters are excluded by the BCECs before transendothelial passage has been completed and hence never reaches the parenchyma [Tai *et al.*, 2009; Zlokovic, 2008].

1.2.3 Receptor and Adsorptive-mediated Transcytosis

Transcytosis of macromolecules across the BBB by endocytotic mechanisms is the main route by which macromolecules enter the brain parenchyma. The majority of macromolecules e.g. hormones and proteins necessary for neuronal function are transported across the BBB by receptor-mediated transcytosis (RMT) [Abbott *et al.*, 2010]. Here a specific transporter is designated to transport a specific macromolecule across the BBB to ensure adequate supply to the brain parenchyma. These transporters can be utilized to develop drug delivery systems targeting the brain by conjugating natural ligands, ligand analogs or antibodies to the delivery system, which targets one of these specific transporters. RMT is a vesicular mediated transport mechanism, where the macromolecular ligands bind to specific receptors on the cell and subsequent the complex is pinched off from the membrane and internalized as a vesicle. The vesicle undergoes transcellular cytoplasmatic transport to the abluminal side of the cell, where exocytosis occurs followed by ligand and receptor dissociation [Abbott *et al.*, 2010]. Several specific transporters have been identified at the BBB, which can be used for targeted drug delivery including but not limited to the insulin receptor [Wu *et al.*, 1997], the melanotransferrin receptor [Demeule *et al.*, 2002], and the transferrin receptor [Friden *et al.*, 1991]. The single most investigated transport system is the transferrin receptor, which is essential for cellular iron uptake (see 1.2.4).

Adsorptive-mediated transcytosis (AMT) is another vesicle mediated transport mechanism. AMT is an uncommon transport system for macromolecules necessary for normal neuronal functioning, but are involved in the transcytosis of macromolecules with a predominantly positive charge, which interact favourable with the glycocalyx of the BCECs membrane. This induces internalization of the macromolecule enveloped in a vesicle and subsequent transcytosis, which proceeds essentially as explained above [Sauer *et al.*, 2005]. Cationized albumin is an example of a protein, which can utilize the AMT pathway to

cross the BBB [Witt *et al.*, 2001]. Although the AMT pathway has a high capacity it is highly unspecific, and cationized drugs will be prone to uptake in all peripheral endothelial cells, making this targeting approach inappropriate for most purposes [Herve *et al.*, 2008].

For both RMT and AMT to succeed the resulting endosome must avoid the lysosomal compartment of the cell to evade degradation. This ability seems to be a specific feature of the BCECs compared to other endothelia [Abbott *et al.*, 2010].

1.2.4 Transferrin/Transferrin Receptor-mediated Transport

In the systemic circulation iron is transported almost exclusively by transferrin under physiological conditions and only in disease states such as hemochromatosis is iron found in a free low-molecular weight form [Moos *et al.*, 2007]. Therefore the iron uptake in cells are dependent on receptor-mediated endocytosis of transferrin [Wang & Pantopoulos, 2011]. The transferrin receptor is a transmembrane disulfide-linked homodimer containing two subunits of 760 amino acids each [Jing & Trowbridge, 1987; Schneider & Williams, 1985]. Transferrin receptors are present on the cell membrane and bind iron-loaded transferrin (iron-transferrin) with high affinity. After binding to its receptor iron-transferrin is internalized in clathrin-coated pits marked with the formation of endocytotic vesicles. Next the pH of the endocytotic vesicles is lowered to 5.5 by an ATP-dependent proton pump in order to reduce the affinity of transferrin to iron, which is essentially irreversible at physiological pH [van Renswoude *et al.*, 1982; Dautry-Varsat *et al.*, 1983]. This event is further facilitated by a membrane bound oxidoreductase, which reduces Fe^{3+} to Fe^{+2} and furthermore assisted by conformational changes in the transferrin receptor [Löw *et al.*, 1987; Bali *et al.*, 1991]. This causes the iron to dissociate from transferrin and the iron is then transported in ferrous form across the endosome and into the cytosol mediated by divalent metal transporter-1 (DMT-1). Next the transferrin receptor is recycled to the cell surface, where a neutral pH promotes the detachment and release of transferrin to the circulation, where it will be reused for additional cycles of iron delivery [Zak *et al.*, 1994]. Although there is a general consensus on the transport cycle of the transferrin-transferrin receptor complex, less agreement exists on iron delivery to the brain mediated by the transferrin receptor.

1.2.5 Iron Transport to the Brain

Iron is essential for growth and normal metabolic function of all mammalian cells. In the brain these functions include cell division, myelination and neurotransmission [Moos *et al.*, 2007]. However the hydrophilic nature of iron prevents its passage to the brain parenchyma, and consequently a transport system must be present, which ensures adequate delivery of iron to the brain. Therefore BCECs exclusively express receptors for transferrin (transferrin receptor-1) on the luminal side. Hence the main mechanism of iron transport to the brain is via receptor-mediated endocytosis in the BCECs. However, a lesser amount is transported to the brain via the choroid plexuses [Crowe & Morgan, 1992] although this uptake is restricted to the parenchyma immediate adjacent to the CSF [Moos, 2002]. Even though a general consensus exists on the uptake of iron-transferrin by transferrin receptors present on the BCECs there's little agreement on the events which follows.

Researchers are divided between different interpretations: I) iron-transferrin is transported through the BCEC by means of receptor mediated transcytosis II) iron-transferrin undergoes receptor mediated endocytosis in BCECs followed by release of iron inside endosomes and subsequent transport of iron into the brain. Iron-free transferrin is then re-endocytosed at the luminal membrane followed by release to the circulation or III) after receptor-mediated endocytosis iron is released from transferrin on the abluminal membrane by the action of citrate and ATP released from astrocytes [Moos *et al.*, 2007]. However research contradicts interpretation I) as the iron transport into the brain greatly exceeds that of transferrin [Crowe & Morgan, 1992; Strahan *et al.*, 1992] and interpretation II) suffers from the fact, that BCECs lack DMT-1 responsible for transport of iron across the endosomal membrane [Moos *et al.*, 2007]. Therefore the most plausible explanation is interpretation III) that the transferrin remains associated with the abluminal membrane releasing the iron without the transferrin detaching from the abluminal membrane and entering the parenchyma [Moos *et al.*, 2007].

1.3 Circumventing the Blood-Brain Barrier

The development of new drugs for CNS disorder is a great challenge and currently there is no effective treatment for the majority of CNS diseases [Lichota *et al.*, 2010; Pardridge, 2005]. Although many new potential therapeu-

tics are available to treat CNS disorders the real challenge is to deliver these compounds across the BBB. Without a drug delivery system only 2 % of small molecular drugs (< 400-500 Da) and 0% of large molecules (> 500 Da) will cross the BBB [Pardridge, 2003]. Multiple approaches have been applied in order to circumvent the BBB and to make drug delivery successful. These approaches can be divided into invasive approaches and non-invasive approaches [Gabathuler, 2010]. The invasive approaches have several disadvantages such as the need for hospitalization of the patients and the risk of complications due to the disruption of the BBB [Gabathuler, 2010]. Therefore non-invasive approaches are investigated as these are more appropriate. Traditionally the non-invasive approaches have focused on optimizing the lead-candidates to posses optimal physiochemical properties, which have led to the development of small molecular drugs and highly lipophilic drugs [Pardridge, 2005]. However these drugs cause no therapeutic benefit in the treatment of severe CNS disorders including neurodegenerative diseases [Pardridge, 2005]. In contrast, several large molecular drugs have shown significant potential for neurodegenerative brain disorders, where the BBB is presumable intact [Astradsson *et al.*, 2009] including proteins like erythropoietin, fibroblast growth factor, glial-derivated neurotrophic factor (GDNF) and brain derived neurotrophic factor (BDNF), small interference RNA's as well as plasmid DNA's [Leist *et al.*, 2004; Kolkova *et al.*, 2000; Lin *et al.*, 1993; Skaper, 2008; Zhang *et al.*, 2003a; Zhang *et al.*, 2003b]. However since these large molecular drugs do not cross the BBB due to their large molecular size and hydrophilic nature, the focus is now turned on nanoparticulate delivery systems including liposomes, polymer-based particles and magnetic nanoparticles [Chertok *et al.*, 2010; Stojanov *et al.*, 2012; Gosk *et al.*, 2004]. These delivery systems can encapsulate or be loaded with therapeutics and be targeted to the BBB by using targeting ligands. Such nanoparticulate systems have great therapeutic potential since they can ferry therapeutics such as proteins or genetic material, which hold great promise in the treatment of CNS disorders [Pardridge, 2005]. However, in order for such drug delivery systems to overcome the BBB, a successful targeting strategy must be employed.

1.3.1 Drug Delivery Targeting the Transferrin Receptor

Transferrin as a CNS drug delivery ligand has a limited value, because almost all transferrin receptors are occupied at physiological conditions due to high endogenous plasma concentrations [Seligman, 1983]. Therefore drug delivery systems utilizing transferrin as a targeting ligand will have to compete with endogenous transferrin for the binding to transferrin receptors. However, as previously mentioned it has been discovered that monoclonal antibodies targeting the transferrin receptors selectively target the BCECs due to a high expression of transferrin receptors exclusively on this endothelium [Friden, 1994; Moos & Morgan, 2001]. In rats OX26 is utilized for targeting the transferrin receptor and binds to an extracellular domain distinct from the binding site of endogenous transferrin, and hence does not compete with endogenous transferrin and nor does it interfere with transferrin associated iron uptake [Jefferies *et al.*, 1984]. Therefore this targeting approach has been investigated as a potential drug delivery system for CNS disorders.

The OX26 targeting paradigm has been exploited in several drug delivery systems and with different cargos. The first study utilizing OX26 conjugated the chemotherapeutic metrotrexate directly to OX26 [Friden *et al.*, 1991]. The loading capacity per OX26 antibody was an average of 6 metrotrexate molecules; however, such a system may experience difficulties reaching concentrations within the therapeutic range.

The most interestingly therapeutics to deliver to the CNS are proteins and genetic material, since these show a high therapeutic potential but still their potential have not been fulfilled due to their high molecular weight and hydrophobic nature, which restrict their passage through the BBB [Lichota *et al.*, 2010]. An approach for conjugating proteins to OX26 transport vectors is the avidin/biotin technology. Avidin, an egg white protein, has four binding sites for biotin per molecule, and even though the binding between avidin and biotin are not covalent it is among the strongest known protein interactions [Green, 1990]. Although the avidin/biotin bond is stable in circulation it becomes labile in tissues, making it ideal for drug delivery [Pardridge, 1999]. The use of the avidin/biotin technology involves biotinylation of the drug and the synthesis of conjugates of OX26 and natural avidin or avidin analogs such as streptavidin. Such conjugates can be prepared by

either chemical linkage of avidin to OX26 or genetically engineering of a OX26/avidin fusion protein. For example conjugates of OX26/avidin with biotinylated BDNF as well as vasoactive intestinal peptide analog (VIPa) have been synthesized by use of the avidin/biotin technology [Pardridge *et al.*, 1994; Bickel *et al.*, 2001; Shin *et al.*, 1997].

Nevertheless, direct conjugation of the drug to the targeting vector by chemical linkage or using the avidin/biotin technology limits the drug-carrying ability of OX26 and chemically modifies the drugs. Therefore a novel-vector based delivery strategy was advised by Huwyler and colleagues by combining liposome technology, PEGylation, and BBB-targeting technology to achieve an efficient drug delivery system [Huwyler *et al.*, 1996]. This approach involves encapsulation of small molecules, plasmids or proteins into the interior of liposomes, and furthermore targeting these vectors to the BBB by conjugating OX26 antibodies to the distal end of PEGylated phospholipids in the liposome wall. These liposomes are known as PEGylated immunoliposomes (PILs). This approach leads to a very high entrapment of small molecules, proteins and plasmids, increasing the carrying capacity of OX26 with as much as 4 logarithmic orders of magnitude for small molecules [Huwyler *et al.*, 1996].

1.3.2 Does OX26 mediate Blood to Endothelium or Blood to Brain Drug Delivery?

Although a clear consensus exists on the matter, that OX26 antibodies can direct blood to endothelium transport [Friden *et al.*, 1991; Moos & Morgan, 2001; Bickel *et al.*, 2001], there are split opinions on whether or not OX26 targeted delivery systems can actually mediate blood to brain delivery and to which extent this occurs. Reviewing 14 articles, which investigate OX26 as a brain targeting ligand 6 of the articles investigated the BBB transport by immunohistochemistry (IHC) (Table 1). However, no immunohistochemial evidence for transcytosis of a OX26 targeted drug delivery system through an uncompromised BBB with subsequent accumulation in the parenchyma was found in any of these articles [Friden *et al.*, 1991; Li *et al.*, 1999; Gosk *et al.*, 2004; Shi & Pardridge, 2000; Moos & Morgan, 2001; Bickel *et al.*, 1994] although several of the articles suggested this in their conclusions (Table 1, see 9-14).

Several investigators have been able to demonstrate targeted delivery using OX26 enhances the brain uptake using a technique known as the capillary depletion technique or measurements on whole brain homogenates. However, analyzes on whole brain homogenates are of limited value since this technique can by no means exclude the possibility of the OX26 targeted delivery system being trapped in the BCECs. Therefore studies using whole brain homogenates to study OX26 mediated drug delivery to the brain utilize inconclusive evidence to draw their conclusions (Table 1, see 1-4 & 10) [Beduneau *et al.*, 2008; Zhang *et al.*, 2003c; Penichet *et al.*, 1999; Huwyler *et al.*, 1996; Li *et al.*, 1999].

The capillary depletion technique involves a density centrifugation step to separate the capillaries from the rest of the brain and can opposed to analyzes on whole brain homogenates be used to quantify the distribution of a test compound between the brain microvasculature and brain parenchyma [Triguero *et al.*, 1990]. However, this technique requires examination of the degree of capillary pollution in the brain fraction in order to correct for this and to check the quality of the separation [Moos & Morgan, 2001]. Unfortunately such a quality control is consistently lagging in the literature, which demonstrates OX26 accumulation in the brain fraction (Table 1, see 5 & 9) [Friden *et al.*, 1991; Cerletti *et al.*, 2000]. However, when Moos and Morgan investigated the brain uptake of OX26 by the capillary depletion technique only 7-9% of the total uptake of OX26 was localized to the brain parenchyma fraction. Quality control was conducted by measuring the alkaline phosphatase activity (BCEC specific enzyme) in both the brain and capillary fraction to ensure proper separation. The investigators found that the OX26 fraction in the brain parenchyma corresponded almost entirely to the fraction of capillary pollution in the brain fraction based on the alkaline phosphatase assay [Moos & Morgan, 2001]. Furthermore these findings were confirmed by a later study (Table 1, see 11 & 12) [Gosk *et al.*, 2004].

	Carrier and administration	Cargo/reporter	Strain	Results, Conclusion and Comments	Reference
	Articles using either capillary depletion technique or measurements on whole brain homogenates				
1	LNC-OX26 LNC- Fab' fragment OX26 LNC-IgG2a (control) *i.v. injection, penile vein*.	Labrafac® containing Radiolabelled ^{188}Re	Adult male Wistar	Radioactivity in whole brain was increased 2 fold and 1.5 fold over non-targeted LNC for LNC conjugated to OX26 and LNC conjugated to OX26 Fab' fragment, respectively. No capillary depletion was performed and no IHC. Therefore the accumulation could be confined to the BCECs.	[Beduneau *et al.*, 2008]
2	OX26-PILs IgG2a-PILs (control) *i.v. injection, femoral vein. 6 consecutive weeks.*	TH Plasmid DNA	Adult male SD rats	Southern blotting on whole brain homogenates for TH plasmid. Detection of TH plasmid only found with OX26-PIL. Conclusion: "The delivery of the TH expression plasmid to brain was verified with Southern blotting". No capillary depletion was performed and no IHC. Therefore the delivery could be confined to the BCECs.	[Zhang *et al.*, 2003c]
3	OX26-Avidin fusion protein *i.v. injection, femoral vein.*	pDNA to reve gene of HIV-1 ^{125}I labelled	Adult male SD rats	The brain uptake of the HIV antisense drug was increased at least 15-fold when bound to the OX26-Avidin fusion protein compared to unencapsulated HIV antisense drug measured by radioactivity in whole brain homogenate. No capillary depletion was performed and no IHC. Therefore the accumulation could be confined to the BCECs.	[Penichet *et al.*, 1999]
4	OX26-PILs *i.v. injection, femoral vein.*	[^{3}H]daunomycin	Adult male SD rats	Radioactivity of whole brain homogenate increased 4 fold when injecting OX26-PIL compared to free daunomycin. Conclusion: "Result indicates that immunoliposomes directed to the brain are trapped in the brain". However, since only daunomycin was radiolabeled it is impossible to comment on the passage of OX26 as well as the liposomes. No capillary depletion was performed and no IHC. Therefore the accumulation could be confined to the BCECs.	[Huwyler *et al.*, 1996]
5	OX26-PILs IgG2a-PILs (control) *Internal carotid artery perfusion for 7 min.*	[^{3}H]daunomycin ^{125}I-labeled OX26 ^{125}I-labeled IgG2a	Rats	Conclusion: "Transcytosis of OX26-immunolipsomes was confirmed in vivo by the brain perfusion and capillary depletion technique". However there was no quality control of the capillary depletion technique and no IHC evidence to support this. No data given for the vascular fraction, but stated that OX26 was absent from this fraction after 7 minutes. This is contradictory to previously literature [Huwyler *et al.*, 1996; Gosk *et al.*, 2004; Friden *et al.*, 1991; Moos & Morgan, 2001] were OX26 was confined to capillary fraction or only present in the brain fraction in a minor amount during the first hour. Hence, the validity of the study can be questioned.	
	Articles investigating OX26 targeted delivery indirectly by outcome in disease models or functional measurements				
6	BDNF-PEG2000-Biotin conjugated to OX26-SA BDNF (control) OX26 (control) *i.v. injection, femoral vein or tail vein.*	BDNF	Adult male SD rats	Stroke model by clamping the common carotid arteries for 12 min followed by i.v. injection immediately after removal of clamp and on daily basis for 1 week on. The neuron density in the C1 sector of the hippocampus was normalized after 1 week. Concluded, that transport across the BBB was enabled by OX26. However the BBB is compromised in this setting and the increased benefit are more likely due to passive extravasation followed by uptake in neurons, which express the transferrin-receptor [Moos, 1996].	[Wu & Pardridge, 1999]
7	^{125}I-bioVIPa ^{125}I-bioVIPa-avidin-OX26 *Intracarotid infusion for 10 min.*	^{125}I radio labelling VIPa	Adult male SD rats	65 % increase in cerebral blood-flow by ^{125}I-bioVIPa-avidin-OX26. However, VIP has been reported to enter the brain parenchyma passively, and thus the increased action of ^{125}I-bioVIPa-avidin-OX26 could be a result of targeted delivery of VIP to endothelial cells where from VIP may be released and pass to the parenchyma [Dogrukol-Ak *et al.*, 2003].	[Bickel *et al.*, 1993]
8	OX26-PILs IgG2a-PILs (control) *i.v. injection, femoral vein*	TH	Adult male SD rats	Unilateral 6-OHDA injections into the right medial forebrain bundle ameliorated the TH activity in contralateral substantia nigra and striatum by degeneration of dopaminergic neurons. Treatment initiated after 4 weeks and consisted of i.v. injection for 7 consecutive days. IHC confirmed restored enzyme activity in the striatum and substantia nigra. TH transcription assayed by RT-PCR on TH	[Zhang *et al.*, 2004]

				mRNA. Conclusion: "The PIL targets the TfR, which causes receptor-mediated transcytosis across the BBB followed by receptor-mediated endocytosis across the neuronal cell membrane". However this disease model suffers from impaired BBB even 4 weeks after surgery and passive extravasation followed by uptake by neurons are a more plausible explanation [Carvey *et al.*, 2005; Moos, 1996].	
	Articles using IHC combined with either capillary depletion technique or measurements on whole brain homogenates				
9	OX26 radiolabeled ^{3}H OX26-MTX conjugate *i.v. injection, tail vein.*	MTX	Female SD rats	IHC demonstrated complete labelling of the capillary bed after 1 hour and after 4 hours a punctuated pattern. Capillary depletion technique showed a preferential accumulation in the vasculature after 1 hour but after 6 and 24 hours this distribution was changed to increased accumulation in parenchyma. No IHC evidence for transcytosis when staining for OX26 or MTX. No quality control was performed for the capillary depletion technique.	[Friden *et al.*, 1991]
10	OX26 ScFv-SA fusion protein Streptavidin-^{3}H-biotin (control) *i.v. injection, femoral vein*	^{3}H-biotin	Adult male SD rats	IHC showed OX26 ScFv-SA fusion protein localized to the vasculature. Radioactivity of in whole brain homogenate increased compared to control. No capillary depletion was performed and IHC confirmed accumulation in the capillaries.	[Li *et al.*, 1999]
11	OX26 IgG2a (control) *i.v. injection, tail vein*	^{125}I-labelled OX26 ^{131} I-labelled IgG2a	P15, P15 iron deficient and P70 Wistar rats	Capillary depletion technique as well as IHC failed to demonstrate OX26 in the brain parenchyma. IHC confirmed complete labelling of the capillaries. The quality of the separation was evaluated with an enzymatic assay for alkaline phosphatase activity.	[Moos & Morgan, 2001]
12	OX26 PIL and IgG2a PIL OX26 and IgG2a (control) *In situ perfusion for 15 min.*	^{125}I-labelled OX26 or IgG2a	P18 Wistar rats	Capillary depletion technique as well as IHC failed to demonstrate OX26-PILs and OX26 in the brain parenchyma. Confocal microscopy confirmed complete labelling of the capillaries by both OX26-PILs and OX26. The quality of the separation was evaluated with an enzymatic assay for alkaline phosphatase activity.	[Gosk *et al.*, 2004]
13	OX26-PILs IgG2a-PILs (control) *i.v.*	32 P-radiolabelled β-galactosidase or non-radiolabeled luciferase.	Adult male SD rats	β-galactosidase histochemistry was performed on brain sections, which were photographed or scanned. Conclusion; widespread transfection of brain parenchyma. However, low magnification and no cell specific counterstaining makes it impossible conclude, which cells where transfected although extensive transfection of the choroid plexus was demonstrated. Luciferase gene expression was analyzed in whole brain homogenate making it impossible to exclude transfection at the capillary level.	[Shi & Pardridge, 2000]
14	OX26-Au UPC1O-Au (control antibody) *Internal carotid artery perfusion for 10 min.*	5 nm colloid gold particles	Adult male SD rats	Electron microscopy on silver-enhanced brain sections revealed, that OX26-Au was present in BCECs reaching the abluminal membrane, however remaining associated with it. Conclusion: "Some gold particles could also be detected on the abluminal plasma membrane of the endothelial cells suggestive of exocytosis". However no OX26-Au could be found in the parenchyma, which would be possible if the OX26-Au was exocytosed at the abluminal membrane.	[Bickel *et al.*, 1994]

Table 1: Review of 14 articles investigating OX26 as a targeting ligand for drug delivery across the BBB. The columns contain information on the carrier and administration form used, the cargo/reporter, strain, results and conclusions made by the authors and comments on this and finally the reference is given. The articles were divided into three categories I) Articles using either capillary depletion technique or measurements on whole brain homogenates II) Articles investigating OX26 targeted delivery indirectly by outcome in disease models or functional measurements and III) Articles using IHC combined with either capillary depletion technique or measurements on whole brain homogenates. Abbreviations: LNC · Lipid nanocapsules. Au · gold. TH · Tyrosine Hydroxylase. SA · Streptavidin. IgG2a · Immunoglobulin isotype G subtype 2a. bioVIPa-avidin-OX26 · biotinylated VIPa attached to OX26-avidin conjugate. OX26 ScFv-SA fusion protein · OX26 single-chain variable fragment (fusion protein of the variable regions of the light and heavy chains with streptavidin)

A common mistake when investigating OX26 targeted drug delivery, is the confounding of OX26 as mediating receptor-mediated transcytosis and thereby enhancing the brain concentration of a therapeutic and/or the treatment efficacy in a disease model; when this is in fact a result of the disease model inducing a compromised BBB or due to increased delivery of the therapeutic compound to the BCECs [Wu & Pardridge, 1999; Bickel *et al.*, 1993; Zhang *et al.*, 2003c]. An example of such a misinterpretation is the investigation of OX26 conjugated PEGylated immunoliposomes (OX26-PILs) as gene delivery vectors. Zhang and colleges subjected rats to unilateral 6-OHDA injections into the right medial forebrain bundle. 6 ODHA is a dopaminergic neuron specific toxin, which therefore ameliorates the tyrosine hydroxylase (TH) activity in the contralateral striatum and substantia nigra. Four weeks later the rats were administered OX26-PILs or IgG2a-PILs containing plasmids coding for TH. Restored TH activity was found in rats subjected to OX26-PIL treatment. The researchers concluded, that restoration of TH activity was achieved through OX26 targeted therapy across the BBB [Zhang *et al.*, 2004]. However no investigation was made to ensure the BBB integrity, which have been demonstrated to be deficient for more than 4 weeks after 6-OHDA injections [Carvey *et al.*, 2005]. The improved efficacy of OX26-PILs over IgG2a-PILs is more likely due to a leaky BBB causing both OX26-PILs as well as IgG2a-PILs to leak from the cerebral microvasculature. However OX26-PILs are much more likely to be taken up by neurons as neurons express transferrin receptors [Moos, 1996].

A peculiar discrepancy is found in studies investigating OX26 targeted brain delivery by both IHC and analyzes on whole brain homogenates or the capillary depletion technique. IHC consistently demonstrates labelling of the microvasculature by the OX26 targeted delivery system but with no evidence of transcytosis. However, when conducting analyzes using whole brain homogenates or capillary depletion technique transcytosis of the OX26 targeted delivery system to the brain parenchyma is consistently reported [Friden *et al.*, 1991; Li *et al.*, 1999; Shi & Pardridge, 2000]. The investigators concluded that OX26 prompted receptor-mediated transcytosis across the BBB. However, as analyzes on whole brain homogenates cannot exclude the accumulation occurs in the BCECs and the capillary depletion technique requires quality control, not used by the investigators, one is left ambiguous towards the findings and conclusions. Furthermore no explanation or reasoning is given to the peculiar lack of immunohistochemical evidence to support such a conclusion.

Thus we, in our research group, are of the opinion that OX26 cannot mediate blood to brain delivery but does successfully mediate blood to endothelium delivery.

1.4 Liposomes as a Drug Delivery System

Liposomes are formed, when a phospholipid film is dispersed in water and agitated. The lipids will form a closed structure with an internal aqueous compartment [Samad *et al.*, 2007]. A unilammelar liposome consists of one phospholipid bilayer where the hydrophilic head groups of the phospholipids are oriented outwards and towards the inner aqueous compartment, respectively. This makes the liposomes water soluble whilst encompassing an inner aqueous compartment (Figure 3) [Samad *et al.*, 2007]. Liposomes are biocompatible and biodegradable vesicles, which can be prepared to carry different cargo and furthermore their size, charge, lipid composition and lammelarity will dictate their field of application [Samad *et al.*, 2007].

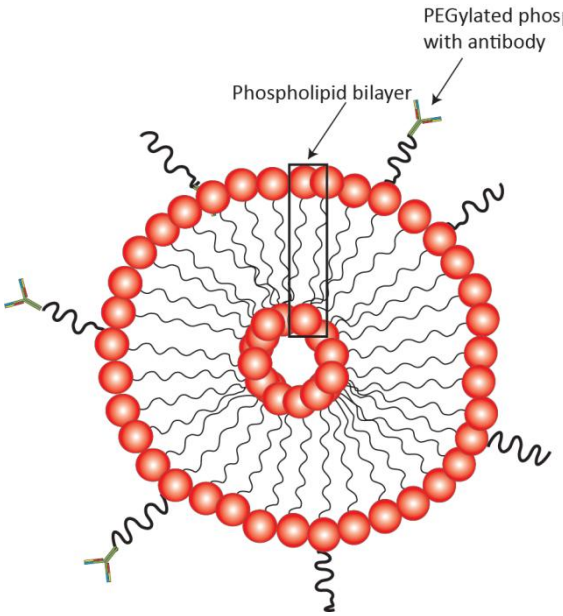

Figure 3: Structure of a unilamellar PEGylated immunoliposome. The liposome wall consists of a phospholipid bilayer with PEGylated phospholipids. The PEGylated phospholipids are functionalized with antibodies for targeted drug delivery. The liposome holds an inner aqueous compartment, which can carry a wide range of therapeutics including proteins and genetic material. *Modified from [Yang, 2010]*

Conventional liposomes are composed of phospholipids and cholesterol, but unfortunately such liposomes suffer from a high plasma clearance due to the reticuloendothelial system (RES). This is a significant obstacle for drug and gene delivery mediated by any particulate system because plasma opsonins as well as complement proteins bind to the particles after i.v. injection [Alam *et al.*, 2010]. This renders them prone to recognition by the Kupffer cells of the liver and macrophages of the spleen, which constitute the RES [Allen, 1994]. A common strategy employed to overcome this obstacle is the use of hydrophilic PEG polymers to decorate the surface of the particulate system. In liposome technology this is most often achieved by incorporating PEGylated phospholipids within the phospholipid bilayer [Allen, 1994]. This approach shields the liposomes and inhibits the binding of plasma opsonins thereby preventing recognition by macrophages of the RES [Schnyder & Huwyler, 2005]. As an example the encapsulation of doxorubicin in PILs, commercial available as Doxil®, resulted in a 50-fold decrease in plasma distribution volume, 200-fold decrease in systemic plasma clearance and 80-fold increase in area under the time concentration curve (AUC) compared to conventional liposomes [Allen, 1994].

Liposomes are convenient for drug delivery purposes, due to their high drug loading capacity. Both hydrophilic, hydrophobic and amphiphilic drugs can be loaded within the liposome. Hydrophobic and amphiphilic drugs will partition into the lipid bilayer whereas hydrophilic drugs will partition in the inner aqueous compartment. The encapsulation of hydrophilic drugs including proteins and genetic material is far less efficient, since the inner volume of the liposome constitute a minor fraction of the total liposome volume [Schnyder & Huwyler, 2005]. An advantage of utilizing liposomes for drug delivery is the fact that drugs loaded within liposomes are protected from metabolic interactions and degradation and furthermore the encapsulated drugs have a better plasma half-life than the non-encapsulated drugs [Sharma & Sharma, 1997; Huwyler *et al.*, 1996].

In order to improve the utilization of liposomes, antibodies can be conjugated to the liposomes in order to yield targeted immunoliposomes. Three types of immunoliposomes can be prepared [Maruyama *et al.*, 1995]; I) the first type is the conventional liposome conjugated with antibodies directly to the surface phospholipids. This yields immunoliposomes, which suffer from the same drawback as conventional liposomes, rapid clearance and therefore reduced benefit from the targeting II) alternatively antibodies can be conjugated to the lipid-bilayer of PILs, which will produce liposomes with a better circulation time. However, the antibodies will be inhibited from connecting from their target because PEG sterically hinders the interaction III) finally antibodies can be conjugated directly to the distal end of the PEGylated phospholipids to yield PILs with long circulation time where the antibodies can interact with their target [Maruyama *et al.*, 1995]. Therefore, this is traditionally the preferred method for preparing PILs.

Usually, PEGylated phospholipids are incorporated into liposomes by including them in the initial lipid composition used for liposome preparation and hereafter functionalized by conjugating antibodies to them. However, this method has some drawbacks, which include random orientation of the functionalized PEGylated phospholipids and the PEGylated phospholipids localized in the inner leaflet of the lipid bilayer will not be accessible for ligand conjugation. One way to circumvent this problem is to use the post-insertion technique [Ishida *et al.*, 1999]. The post-insertion technique involves the preparation of a micelle mixture containing PEGylated lipids and conjugating antibodies directly to the micelles. The functionalized PEGylated lipids can afterwards be inserted into preformed liposomes, by incubating preformed micelles and liposomes together at a temperature above the phase transition temperature of the lipids. PILs prepared by the post insertion technique have been demonstrated to have ligand densities and in vivo performance characteristics similar to PILs prepared by the traditional approach [Iden & Allen, 2001].

OX26-PILs have been extensively investigated as a drug-delivery system for the CNS. However, the literature is as described in section 1.3.2 contradictory.

1.5 Magnetic Responsive Drug Delivery Systems

The magnetic properties of MNPs can be utilized in a multitude of applications. In vitro applications include; cell sorting, purification and transfection, whereas in vivo applications are drug delivery, gene delivery, hyperthermia treatment and magnetic resonance imaging (MRI) or a combination of the above [Namdeo *et al.*, 2008]. Most

attention has been given to drug and gene delivery due to the significant advantages of magnetic susceptible drug carriers. The concept of utilizing MNPs for drug delivery was introduced in the 1970s by Senyei and colleges, who proposed that therapeutic agents could be attached to or encapsulated within MNPs. In order for such a delivery system to constitute an ideal magnetic responsive drug carrier the authors proposed six criteria, which should be fulfilled [Senyei *et al.*, 1978]:

- Size of less than 1.4 µm
- Adequate magnetic responsiveness
- Capacity to carry a wide range of therapeutics
- A controllable and predictable release of the therapeutic at the target site
- A surface coating with high biocompatibility and minimal antigenicity
- The degradation products should give rise to minimal or no toxicity

Based on these criteria, a large range of MNPs have been designed for a multitude of applications [Namdeo *et al.*, 2008].

1.5.1 Structure of Magnetic Nanoparticles

The basic structure of a MNP is a centrally located magnetic core (Figure 4). Although one can think of a magnetic carrier composed exclusively of a magnetic core, such a carrier is of limited utility due to low drug loading capacity, uncontrolled release and shortage of functional groups, which limits the usage for most therapeutic applications [Namdeo *et al.*, 2008]. Thus, the magnetic core is surrounded by a protective coating, which can be functionalized by attaching a diverse range of molecules [McBain *et al.*, 2008]. In the majority of cases the core is made of superparamagnetic iron oxide either magnetite (Fe_3O_4) or maghemite (γ-Fe_2O_3). The MNPs shows magnetic properties only during magnetization, which allows an external magnet to control the movement of the particles, and loose them when the magnetic field is removed [Namdeo *et al.*, 2008; Alexiou *et al.*, 2006]. This property is used in order to direct the particles to the target site for local delivery. For in vivo applications the size of the MNPs is an important factor in order to allow for sufficient magnetic targeting. As a result a magnetic core with a hydrodynamic diameter of approximately 100 nm is usually employed. The magnetic core consist of conglomerates of single iron oxide domains with sizes of 10-15 nm, since single domain iron oxide particles are not attractable against the blood flow in vivo [Alexiou *et al.*, 2006]. The most studied material for the magnetic core is magnetite, and since magnetite has been found to exhibit a very low toxicity, it is the favoured core material [Namdeo *et al.*, 2008].

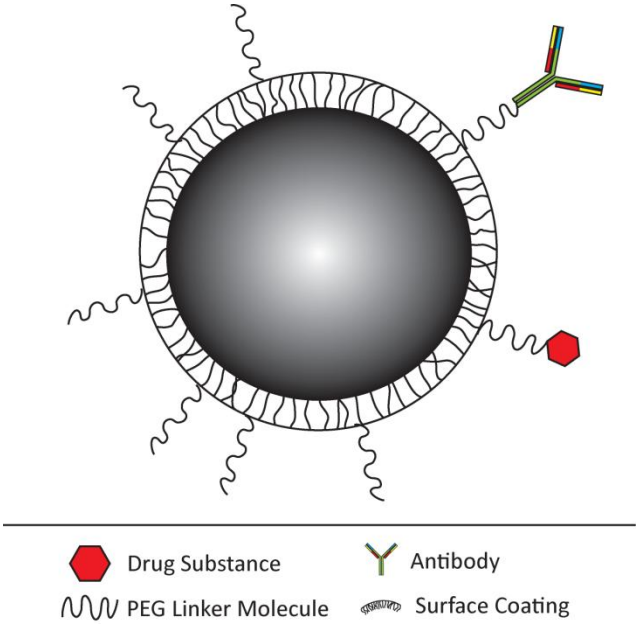

Figure 4: General structure of a MNP. A centrally located magnetic iron oxide core is coated in a polymer surface coating. The coating can be functionalized by PEGylation and conjugation of drug substances or antibodies can be conjugated directly to the surface coating or to the PEG-molecules as shown in the figure

The surface coating is a pivotal component of the MNPs, as it provides the particles with their unique features and capabilities. The surface coating should ideally I) stabilize the particle suspension to avoid agglomeration II) be biocompatible and biodegradable III) provide a stealth function for in vivo applications, in order to shield the particles from serum proteins and protect them from capture by the RES thereby prolonging the circulation time IV) finally the surface coating should provide functional groups for the specific demands of the delivery system e.g. cationic groups for DNA complexation and condensation for gene delivery [Alexiou *et al.*, 2006]. Hence, the surface coating is a crucial component for designing MNPs, which exhibits high therapeutic efficacy as well as safety.

The advantage of using a magnetic susceptible drug-carrier with a functionalized coating can be summarized as I) the ability to target specific tissues as a result of magnetic targeting and a functionalized coating II) a reduction in the drug quantity needed to reach a therapeu-

tic concentration and III) a reduction of adverse effects as a result of a reduced drug load outside the target site.

1.5.2 Structure of Magnetoliposomes

An alternative system for drug delivery opposed to regular MNPs is a system based on combining magnetic nanoparticle technology and liposome technology [Martina *et al.*, 2005]. This hybrid nanoparticle platform shares the magnetic properties of the MNPs and combines it with the advantages of liposomes including, no cellular toxicity, biological stability and avoidance of uptake by the reticuloendothelial system [Martina *et al.*, 2005]. MLs consist of MNPs encapsulated in a phospholipid bilayer and principally two strategies can be employed in order to produce MLs (Figure 5).

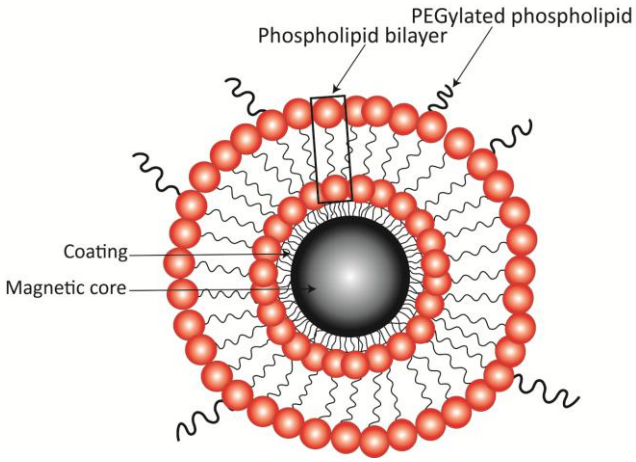

Figure 5: Structure of a ML depicting a centrally located magnetic core with a surface coating. The magnetic core is enveloped by a phospholipid bilayer containing PEGylated lipids.

The first method is direct absorption of lipids onto the surface of the magnetic nanoparticle. This results in 100% encapsulation; however, at the expense of any internal aqueous compartment making it virtually impossible to incorporate any hydrophilic molecules within the MLs and thereby obliterating their therapeutic potential for most applications [Martina *et al.*, 2005]. The second method for producing MLs consists of creating a dry lipid film and hereafter hydrating it in the presence of a magnetic fluid. This will produce MNPs enveloped in large liposomes, which consist of multiple layers. Ultrasonification and or extrusion through filters may reduce their lamellarity and size. However this approach will always yield some unencapsulated magnetic fluid [Martina *et al.*, 2005].

1.5.3 Studies using Magnetic Responsive Drug Delivery Systems

Targeting using magnetic forces have been investigated in patients with advanced cancer and have been well tolerated [Lubbe *et al.*, 1996b; Lubbe *et al.*, 1996a; Alexiou *et al.*, 2000; Alexiou *et al.*, 2003]. These studies investigate micrometric magnetic particles but these particles suffer from a high clearance and resultant low plasma half-life [Rivière *et al.*, 2007]. Thus, nanometric MLs may serve as improved delivery system over magnetic particles, because their clearance can be reduced significantly by the phospholipid bilayer and incorporation of PEGylated phospholipids. Such MLs have been demonstrated to still remain in circulation for more than 24 hours [Martina *et al.*, 2005]. Such circulation times are difficult to achieve with MNPs, even if their surface is stabilized with PEG. For example a study on cationic MNPs with and without PEG-chains showed that PEG had a dramatic impact the AUC increasing it by 11 fold. However, the particles were virtually absent from the circulation within 10 minutes [Chertok *et al.*, 2009]. Compared to this result cationic MLs have also been injected i.v. in mice, and after 24 hours some MLs were still present in the plasma [Dandamudi & Campbell, 2007]. Dandamudi and colleges studied cationic MLs to target melanoma tumours in mice. The setup involved injection of cationic MLs while placing a 1.2 T magnet over the external surface of the tumour and resulted in a 2-fold retention of cationic MLs after 2 hours [Dandamudi & Campbell, 2007]. Melanoma is an ideal disease model for magnetic targeting due to its superficial location. This highlights an important aspect of magnetic drug targeting, which still remains a hurdle. While effective magnetic targeting is feasible for organs near the body surface, organs deeper within the body are difficult to target since the magnetic field strength decays exponentially with increased distance to the magnet. Some investigators have circumvented this problem by implanting magnets near the target site [Kubo *et al.*, 2000; Forbes *et al.*, 2008].

Although both MNPs and MLs can serve as potential and beneficial drug delivery system for CNS disorders, not much attention has been given to these delivery systems. The primary focus of these drug delivery systems has been in different tumour models both for drug delivery, gene delivery and imaging [Alexiou *et al.*, 2006]. MNPs have for example been investigated as a delivery system for glioblastoma multiforme; however, such diseases have

a leaky capillary network, which give rise to a passive targeting due to enhanced permeation and retention of the particles [Chertok *et al.*, 2009; Chertok *et al.*, 2010]. Only few studies have investigated if magnetic susceptible delivery systems under the influence of an external magnetic field can cause delivery across the BBB. Rivière et al. investigated this by injecting MLs i.v. and monitoring the MLs using laser-scanning confocal fluorescence microscopy through a cranial window in live mice. They found that 15 minutes after i.v. injection, with an external magnet placed over the brain, MLs were generally trapped within cerebral venules but there were no evidence to support passage of the BBB [Rivière *et al.*, 2007]. However, their MLs were composed of a phospholipid bilayer with no active brain targeting strategy and therefore, it might be expected that the particles did not traverse the BBB.

Another study performed by Qiao et al. compared PEG-coated MNPs with or without the BBB targeting ligand lactoferrin. They evaluated the potential of these particles to cross the in vitro BBB made by primary porcine brain capillary endothelial cells, and found that lactoferrin targeting significantly improved the permeation [Qiao *et al.*, 2012]. However the unconjugated particles also passed through the in vitro BBB in a considerable amount. In fact 22% of the unconjugated particles were present on the "brain side" of the in vitro BBB compared to 47% of the lactoferrin conjugated particles. The particles were also tested in vivo by i.v. injection, and retention and permeation was measured by magnetic resonance imaging (MRI), where MNPs will show enhanced MR contrast on MR images. Significant enhanced contrast was found for both particles in MR images of the brain 24 hours after injection. However contrast in the temporal cortex was even higher for unconjugated particles than those conjugated with lactoferrin, although lactoferrin conjugated particles showed increased retention in the thalamus, brain stem and frontal cortex. However, MRI cannot prove transcytosis across the BBB and due to the fact that no other investigations were performed it remains elusive if such particles were able to pass the BBB. The authors did furthermore not investigate whether the retention in the brain could be improved by magnetic targeting [Qiao *et al.*, 2012]. To this date no studies have investigated if a combinational approach with magnetic guidance by an external magnetic and OX26 targeting can direct the traversal of MLs across the BBB.

2. Materials and Methods

2.1 OX26 Hybridoma Cell Line Culture, Antibody Production, Purification and Testing

2.1.1 Culture and Antibody Production

OX26 hybridoma cells (HPA culture collection, 84112014) were cultured in RPMI 1640 medium (Sigma Aldrich, RO883) supplemented with 10% Fetal Calf Serum, 2 mM glutamine, 0.04 mg/ml gentamycin with HAT (100 µM hypoxanthine, 0.4 µM aminopterin and 16 µM thymidine) at 37°C, 5% CO_2 in a humidified atmosphere. The OX26 hybridoma cells were initially seeded into a 96 well plate at different densities by serial dilution. In order to facilitate resuscitation of the OX26 hybridoma culture peritoneal macrophages were acquired from one balb/c mice by injecting RPMI 1640 medium intraperitoneal and then withdrawing the medium. The medium containing the macrophages was then divided between the wells. Hereafter, the viability of the hybridoma cell culture was observed, and wells with high viability were selected for subculturing. Subculturing was continued, until the cell count was sufficient for culture in two T175 culturing flasks. When the confluency reached 70% the cells were subcultured into a CELLine™ CL1000 Bioreactor (BD Biosciences™, 353137). Concurrently with subculturing into wells or flasks with a higher surface area, the medium's serum concentration was steady decreased until the concentration was 1%. The cells did not remain viable if total serum withdrawal was performed. The serum reduction was performed in order to reduce the amount of foreign proteins, which were of no interest in the final antibody purification.

The CELLine™ CL1000 Bioreactor is a novel culturing system, which allows the production of monoclonal antibodies with a high yield and concentration (Figure 6). The cells are maintained in a cultivation chamber, which is separated from the nutrient supply chamber by a semi-permeable membrane allowing amino acids, sugars, salts and other nutrients to pass the membrane. The antibodies secreted in the cultivation chamber are not allowed to pass due to the membrane's low molecular weight cut-off, which is 10,000 Dalton. The cells rest on a silicone membrane, which allows direct asses to oxygen and rapid removal of carbon dioxide. Access to the nutrient and cultivation compartments is available through separate ports.

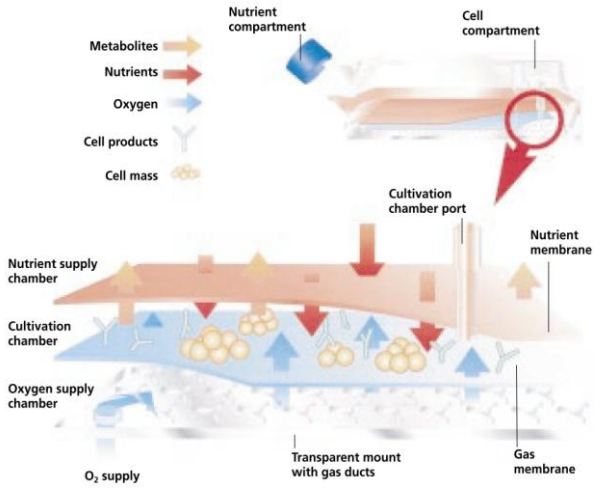

Figure 6: Schematic view of the CELLine™ CL1000 Bioreactor. The cultivation chamber is separated from the nutrient supply chamber by a semi-permeable membrane, which allows passage of nutrients but restricts the passage of the antibodies. The cells rest on a silicone membrane, which allows free passage of oxygen and carbon dioxide. Separate ports allow asses to the nutrient and cell compartment.

Figure from BD Falcon™ Manual.

The medium was changed to ProDoma™ medium (Lonza, BEO2-029Q) supplemented with 1% FCS, when culturing in the CELLine™ CL1000 Bioreactor and the medium was renewed once every week. Concurrent with the medium renewal the medium from the cultivation chamber containing the antibodies was removed. Clarification of the medium by centrifugation was done in order to remove bulk proteins, dead cell debris and particulate matter, which could later interfere with the purification by clogging the column. Clarification was done by spinning down the medium at 2000 rpm for 5 min. Next the supernatant was added to a falcon tube and transferred to the -83°C freezer.

2.1.2 Antibody Purification

GE-healthcare, XK-column 16 was packed with protein G Sepharose gel (Gammabind™ Plus Sepharose, 17-0885-01) dissolved in binding buffer consisting of 1M glycine, 0.15M NaCl, pH 8.5. Four weeks antibody harvest was filtered through a 0.22µm filter to remove any remaining bulk proteins, dead cell debris and particulate matter. Hereafter, the supernatant was mixed 1:1 with binding buffer. A sample was taken from this, which is referred to as the zero-sample and next the suspension was run on the column with a flow rate of 1 ml/min, and an additional sample was collected from the flow-through. Finally binding buffer was run on the column to remove all unbound material, and a sample was taken before beginning the elution. Next the antibodies were eluted from the column by running elution buffer consisting of 0.1 M glycine, pH 2.7 through the column and collected in 2 ml fractions and neutralized by adding 10% v/v 1M Tris-HCl, pH 9.0. The absorbance at 280 nm was measured with a spectrophotometer (Thermo Scientific, Genesys 10UV Scanning) for each elution fraction to generate an elution diagram.

The elution fractions were next loaded and run on 16% sodium dodecyl sulfate (SDS) gel and proteins were visualized with Coomassie stain in order to determine the purity of the elution fractions. All elution fractions were added diluted 15 times in HEPES-buffer mixed in the ratio 1:1 with Laemmeli sample buffer (Sigma Aldrich, S3401) and denatured by heating to 95°C for 5 min, loaded into the wells of a 16% SDS gel (Run Blue, NXG01612) and run in Rapid SDS Run Buffer (Run Blue, NX14500) for 1 hour at 150V. Finally the gel was stained with Coomassie stain (0.2% w/v Coomassie Brilliant Blue R250 in a solution of 50% ethanol 20% acetic acid and 30% distilled water) for 10 minutes, washed three times in distilled water, and left in destaining solution (10% ethanol and 7.5% acetic acid in distilled water) overnight with a piece of sponge to absorb the Coomassie stain.

Dialysis of selected elution fractions was performed with dialysis tubing, Spectra/Por 1 with MWCO of 6-8 kDa (Spectrumlabs, 132650), in order to remove any amines from the sample, which could later interfere with the conjugation. The dialysis tubing was rinsed by bathing in 1L ddH_2O overnight to remove any pollutants from manufacturing and preservatives. Next the tubing was filled with the sample and closed with dialysis tubing closures. Finally the tubing was transferred to a beaker glass with a sample to dialysate ratio of 1:100 v/v. HEPES-buffer was used as dialysate, which consisted of 136 mM NaCl, 10 mM HEPES and 1 mM EDTA. The dialysate was renewed after 4 hours and prior to leaving overnight. Next day the sample concentration was determined as described in section 2.4.2, divided into aliquots, and stored at -20°C until further use.

2.1.3 Antibody Testing

In vitro testing on RBE4 cells

Immunocytochemistry was performed on immortalized rat brain endothelial cells (RBE4 cells) cultured in 8 well chamber slides (Permanox®, 177445) in order to test the OX26 antibodies affinity towards the target tissue. OX26 antibodies were tested on RBE4 cells in three different dilutions 1:100, 1:200 and 1:400 against mouse anti-rat anti-CD71 antibodies (anti-CD71 antibodies) (Serotec, MCA155R), which also show affinity towards the rat transferrin receptor.

RBE4 cells were first fixed in 4% paraformaldehyde for 15 minutes. Next cells were incubated in incubation buffer (3% swine serum, 0.03% Triton-X in KPBS) for 30 minutes followed by addition of the primary antibody in the aforementioned dilutions and incubated for 1 hour. Wells were washed three times in KPBS between each step. Next the secondary biotinylated antibody goat anti-mouse (DAKO, E0464) was added diluted 1:200 in incubation buffer and incubated for 30 minutes. Finally the fluorescent label streptavidin Alexa Fluor® 488 (Invitrogen, S32354) was added diluted 1:200 in incubation buffer and incubated for 30 minutes. Finally nuclei were counterstained with DAPI (2µg/ml) and placed under coverslips with fluorescence mounting medium (DAKO, S3023).

In vivo testing of OX26

In vivo affinity towards the BCECs was tested by giving an i.v. bolus injection of 200 µL containing 300 µg OX26 antibody in the lateral tail vein of a Wistar rat (n = 1). After two hours organs were excised and treated as described in section 2.6.3. In addition all organs from a Wistar rat (n = 1), which did not receive any OX26 were excised and served as a negative control.

2.2 RBE4 Cell Culture

RBE4 cells were cultured in a growth medium consisting of 50% Alpha-MEM with Glutamax-1 (Gibco, 32-561) and 50% HAM's F-10 with Glutamax-1 (Gibco, 41-550) with supplementary 10% Fetal Calf Serum, 1% Penicillin-Streptomycin (Gibco, 15140-122), 300 µg/mL Geneticin Sulfate (Acros Organics, 32940-0010) and 1 ng/mL basic Fibroblast Growth Factor (Invitrogen, 13-256-029). The medium was renewed every 2-3 days and the cells were cultured at 37°C, 5% CO_2 in a humidified atmosphere (Holm and Halby, IGO 150 cell life).

2.3 Particle Synthesis

2.3.1 Synthesis of Magnetoliposomes

Lipid-encapsulation of starch-coated MNPs marked with a red fluorescent dye (S-MNPs) (Chemicell, 4418-1) was performed based on the method presented by Dandamudi *et al.* in order to produce MLs (Figure 7 & Figure 8) [Dandamudi & Campbell, 2007]. Briefly, a lipid mixture consisting of L-α-phosphatidylcholine (Soy PC) (Avanti, 840072), Dimethyldioctadecylammonium bromide (DDAB) (Sigma, D2779-10G), and 1,2-dipalmitoyl-sn-glycero-3-phosphoethanolamine-N-methoxy(polyethylene glycol)-2000] (mPEG2000-PE), all dissolved in chloroform, was prepared in a mole ratio of 37:60:3, respectively. This lipid suspension was dried into a thin lipid film in a round-bottom bottle, under a continuous stream of nitrogen gas. After evaporation, the resulting lipid film was further exposed to a stream of nitrogen gas for 30 min to ensure complete evaporation of the organic solvent. The resulting lipid film was rehydrated in HEPES buffer consisting of 136 mM NaCl, 10 mM HEPES, and 1 mM EDTA, containing the MNPs in a w/w ratio of 1:10 (MNPs/solid lipid). A typical batch consisted of 3 mg S-MNPs to 30 mg lipids (11.25 mg Soy PC, 3.45mg mPEG2000-PE and 15.3 mg DDAB). Next the lipid film was immediately vortexed until completely dissolved, whereafter the mixture was placed on a belly dancer and incubated at ambient temperature for 1 hour to allow complete rehydration. Next, the mixture was placed in a water bath and extensively sonicated (Bransonic, 1510E-DTH) for 1.5 hour to break up any lipid aggregates and to promote the formation of unilamellar liposomes. Excess lipid was then removed by three times magnetic decantation using a DynaMAG™-2 magnet (Invitrogen, 123-21D), followed by resuspension in 1.5 ml HEPES buffer and finally the resulting MLs were characterized as explained in section 2.4 and stored at 4°C for a maximum of 3 days.

2.3.2 Preparation of Micelles

Micelles were prepared by mixing 1,2-distearoyl-sn-glycero-3-phosphoethanolamine-N-[maleimide(polyethylene glycol)-2000] (DSPE-PEG2000-maleimide) (Avanti Polar Lipids, 880126P) and mPEG2000-PE in a molar ratio of 4:1. A typical batch consisted of 2.94 mg DSPE-PEG2000-maleimide and 0.69 mg mPEG2000-PE. Lipids dissolved in chloroform were transferred to a round-bottom flask and dried into a thin lipid film, under a continuous stream of nitrogen gas until no visible solvent was

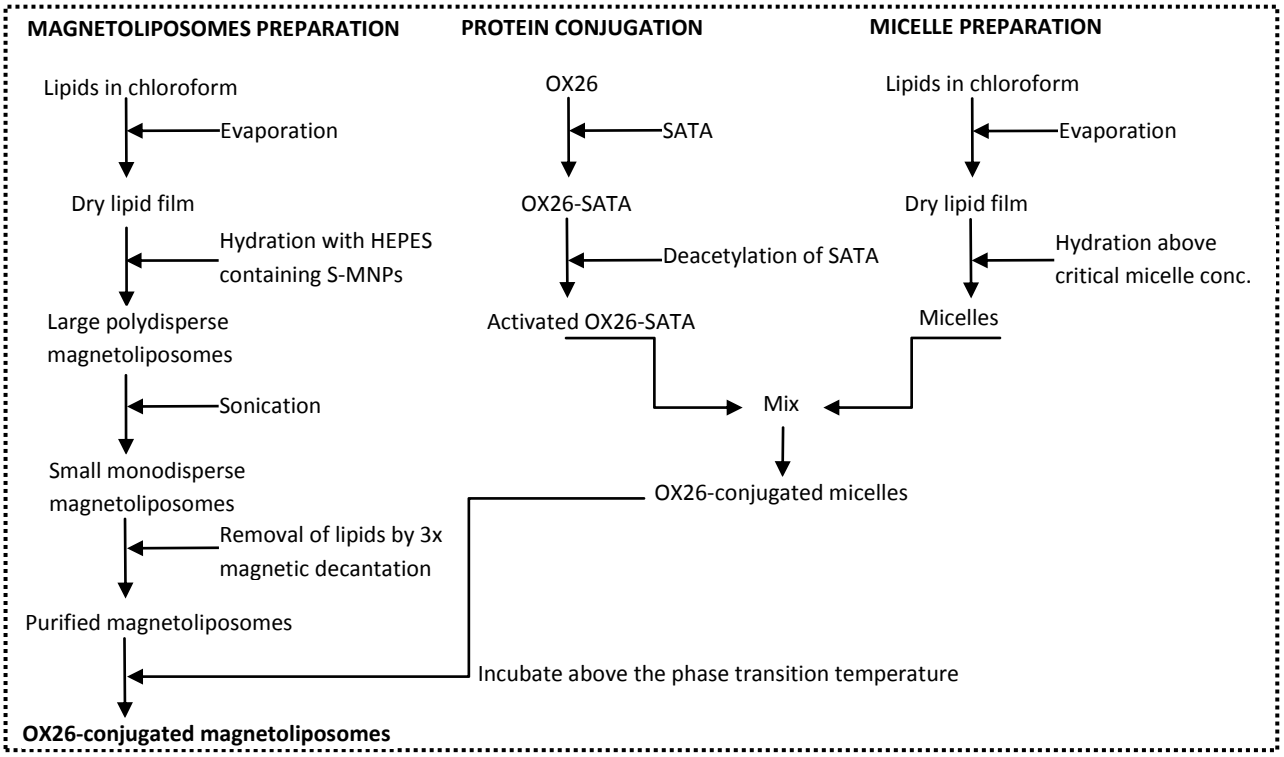

Figure 7: Schematic overview of OX26-ML synthesis. The synthesis consists of three separate processes; I) preparation of magnetoliposomes by lipid film hydration and sonication, II) modification of OX26 with SATA and III) preparation of micelles containing maleimide-functionalized lipids. The micelles are conjugated with the activated SATA-modified OX26 and post-inserted into preformed magnetoliposomes to yield OX26-MLs.

left. The evaporation was then continued for additional 30 min to ensure complete evaporation of the organic solvent. The resulting lipid film was rehydrated in HEPES buffer preheated to 65°C and the lipid film was immediately vortexed until it was completely dissolved. The final lipid-concentration was 10 mM in order to exceed the critical micelle concentration of the two lipids. Micelles were formed by heating the lipids to 65°C during continuous agitation for 1 hour at 1400 rpm in a Thermomixer (Eppendorf Nordic ApS, AH Diagnostics)

2.3.3 Conjugation of Antibodies using the SATA-method

The monoclonal mouse anti-rat transferrin receptor antibody OX26 was used for the preparation of OX26-MLs. SATA-conjugation was performed by dissolving SATA in N-N dimethylformamide (10 mg SATA/ml) and then mixing the SATA-solution with OX26-solution in a molar ratio of SATA:OX26 8:1. The mixture was incubated for 45 minutes at ambient temperature during continuous rotation on a belly-dancer. Free SATA was removed by using a Vivaspin 6 ultrafiltration column with a molecular weight cut-off of 50 kDa (GE healthcare, 28-9323-18) using the manufacturer's instructions and the OX26 antibodies were resuspended in HEPES-buffer. The protein concentration was determined using UV-function on a spectrophotometer (Implen nanophotometer™), and the modified antibodies were stored at -20°C until use. Before conjugation of OX26 to micelles the SATA groups were deacetylated in order to create free sulfhydryl groups to react with the maleimide group in the micelles. Deacetylation was performed by adding a freshly prepared hydroxylamine solution (0.5 M hydroxylamine HCl, 0.5 M HEPES, and 25 mM EDTA) to the OX26 solution in a 1:10 v/v ratio and incubated for 1 hour at room temperature during continuous rotation. Conjugation was performed by mixing deacetylated OX26 with micelles in a molar ratio of 1:10 for OX26:DSPE-PEG2000-maleimide and incubating the solution for 2 hours at room temperature and then overnight at 4°C on a belly-dancer.

2.3.4 Antibody Transfer - Synthesis of OX26 conjugated Magnetoliposomes

OX26 conjugated micelles were mixed with MLs in a w/w ratio of MLs to micelle phospholipids of 1:1.25. The suspension was heated to 60°C for 1 hour during continuous rotation at 1400 rpm in a Thermomixer and then cooled down to room temperature. Next unbound OX26 and

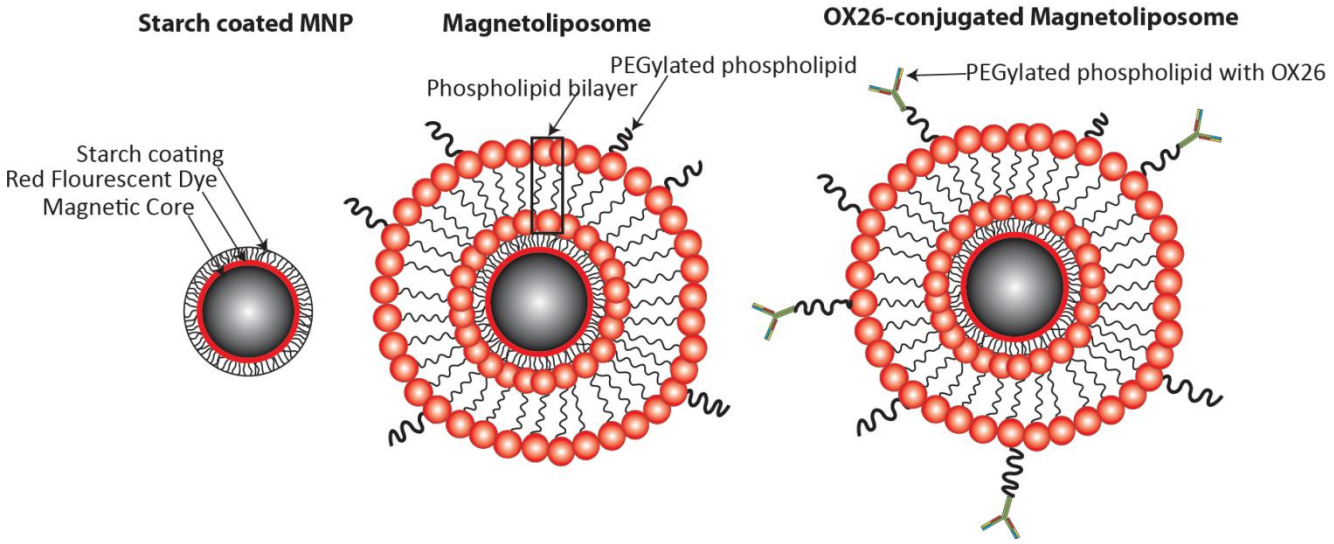

Figure 8: Schematic structure of the three particle types used in the present study. The S-MNPs consist of a superparamagnetic iron oxide core made of magnetite coated by starch and marked by a red fluorescent dye with an excitation of 578 nm and emission of 613 nm. The MLs consist of S-MNPs enveloped in a phospholipid bilayer with PEGylated phospholipids. The OX26-MLs are essentially MLs but with OX26 functionalized PEGylated phospholipids.

micelles were removed from the sample by magnetic decantation of the suspension and removal of the supernatant twice. The OX26-MLs of a typical batch were finally resuspended in 1.5 ml HEPES-buffer.

2.3.5 Determination of the Particle Concentration after synthesis

The concentration of MLs and OX26-MLs were determined after synthesis based on a previously described iron quantification approach [Boutry *et al.*, 2009]. The quantification of MLs and OX26 MLs was expressed as µg of S-MNP present in the samples. The approach is based on the Perl's Prussian Blue reaction, which allows for blue-staining of iron-containing solutions, when digested in hydrochloric acid and potassium ferrocyanide. Ferrocyanide reacts with ferric chloride to form ferric ferrocyanide, which is a blue coloured colloidal complex with a large absorption band centred around 700 nm [Boutry *et al.*, 2009].

A standard curve was initially established from the S-MNPs provided by diluting 1, 2, 4, 6, 8, 10 and 12 µg of the S-MNPs in 100 µL of HEPES-buffer. Next 200 µL 5M HCl was added to each standard and treated for 4 hours at 80°C in a thermomixer at 450 rpm. Finally 100 µL of 5% aqueous solution of ferrocyanide was added and incubated at room temperature for 15 minutes, and hereafter the absorbance at 650 nm was measured with a spectrophotometer (Thermo Scientific, Genesys 10UV Scanning).

In addition to the standards, three samples of both MLs and OX26 MLs was taken from the synthesized stocks and treated in the same manner as the standards. A standard curve was next generated from the standards, and the concentration of the MLs and OX26 MLs was determined using the standard curve generated in Microsoft Excel 2007.

2.4 Particle Characterization

2.4.1 Determination of the Size and Zeta-potential

Mean particle size and charge were assessed using a Zetasizer Nano ZS (Malvern). The mean particle size was determined by dynamic light scattering and the zeta potential was determined by laser doppler electrophoresis. All measurements were performed on three separate samples suspended in HEPES-buffer in order to ensure reproducibility and data was analyzed using Malvern Zetasizer Software v. 6.2.

2.4.2 Determination of Antibody Concentration

The concentrations of antibodies were determined using the RC DC Protein Assay (Bio-Rad, Denmark), which is based on the Lowry assay. The reaction mechanism is not completely understood but involves the oxidation of aromatic aminoacids catalyzed by copper, and the assay is therefore dependent on the proteins content of aromatic aminoacids [Lowry *et al.*, 1951]. The reaction gives of a

chromogenic compound, reduced folin, which was measured by absorbance at 750 nm with a spectrophotometer.

The assay was carried out according to the manufacturer's microfuge tube assay protocol. A standard curve was made with 5 dilutions of human serum IgG (Sigma Aldrich, 56834) in HEPES-buffer in the range of 0.2-1.5 mg/ml. The antibody concentration in the samples was diluted to make sure it was within the range of the standard curve. Furthermore for determining the OX26 concentration in OX26-MLs batches the absorbance of an equivalent amount of MLs were subtracted to correct the measured absorbance of OX26-MLs. Next a best-fit linear regression was made and the antibody concentration was calculated (Microsoft Excel 2007).

2.5 In vitro Binding and Uptake Assay

RBE4 cells were seeded in 8 well Permanox® chamber slides (0.8 cm^2 /well) at a density of 30,000 cells/cm^2 and cultured for 24 hours. Medium was aspirated and fresh medium added. Next S-MNP, MLs and OX26 MLs were added to separate wells with 1µg, 2µg, 3 µg, 4 µg and 5 µg per well, respectively, and incubated for 3 hours. Unbound particles were then removed by washing three times with PBS followed by fixation of the cells for 15 minutes with 4 % paraformaldehyde and finally DAPI-stained with a working concentration of 2µg/ml before being mounted under coverslips with fluorescent mounting medium.

Quantitatively measurements on the particle uptake was assesed based on a method presented by Shigeoka [Shigeoka *et al.*, 2007]. The mean fluorescence intensity of each individual cell in image 15A, B and C were assessed in ImageJ v. 1.45s using a free hand selection tool. Furthermore the median fluorescence intensity for all cells were calculated in SPSS and displayed in a bar plot. Statistical analyze was carried out in SPSS (SPSS, 2012). Since the variances could not be assumed to be equal between groups one-way ANOVA was not utilized. Therefore non-parametric tests were used. The Mann-Whitney-U test was used to determine, which groups were significantly different from each other ($p < 0.05$)

2.6 Experiment Animal Work

Animals were kept in a room with a 12 hour light / 12 hour dark schedule. The animals were allowed free access to food and water. The daily care of the animals was performed by the staff at the animal facility at Sygehus Nord, Aalborg, where all the animal experiments were carried out. All surgical procedures were approved by Rådet for Dyreforsøg under the Danish Ministry of Justice.

2.6.1 Biodistribution Experiment

In vivo biodistribution of MLs (n = 2) and OX26-MLs (n = 2) was studied in P16 Sprague Dawley (SD) rats, which received a single bolus injection of 10 µg/g bodyweight administered by i.v. injection in the lateral tail vein. 24 hours after administration the rats were deeply anesthetized by intraperitoneal injection of 0.5 ml of Avertin®, absence of tail and paw withdrawal reflexes were checked, rats were then transcardial in situ perfusion fixed with 4 % formalin and finally all organs were removed. Organs were handled and sectioned as described in section 2.6.3.

DAPI-staining of tissue sections was performed free-floating in Nunc™ containers in a working solution of 2 µg/ml DAPI diluted in PBS, after which sections were rinsed three times with PBS. Finally the sections were transferred onto superfrost slides and allowed to air dry before being placed under coverslips with Pertex mounting media. Fluorescence images were acquired as described in section 2.7.

2.6.2 In situ Brain Perfusion

In situ brain perfusion (ISP) was performed on deeply anesthetized P16 SD or Wistar rats. The perfusion was performed transcardially with a peristaltic pump (Minipuls 3, Gilson). Initially the thorax was surgical opened and the thorax wall removed. Next the right atrium was opened with a surgical scissor, followed by insertion of a G23 needle (Terumo, 56834), connected to the peristaltic tubing, into the left ventricle. Initially the circulatory was perfused for 30-45 seconds with isotonic saline with 100 IU/mL heparine (LeoPharma) in order to prewash the circulatory system and avoid blood clotting. The perfusion was then continued at 5 ml/min for 15 minutes with perfusion medium consisting of M199 medium (Gibco, 3849059.), containing either MLs or OX26-MLs. The M199 medium was kept at 37°C by placing it in a water bath (Elmi, TW-2) and continuously oxygenated by bubbling 100% O_2 into the medium. Two variables were present in this setup, particle type and the presence or absence of an extracranial placed magnet. The rats always received 10 µg/g bodyweight independent of particle type. The magnet used for the experiments was a 1.40-1.46 T neo-

dymium magnet and was placed extracranial in intimate contact with the scalp of the rats.

- Group 1, n = 6 received OX26-MLs with magnetic field manipulation.
- Group 2, n = 1 received OX26-MLs without magnetic field manipulation.
- Group 3, n = 2 received MLs with magnetic field manipulation
- Group 4, n = 1 received MLs without magnetic field manipulation.

After the experiment was finished the circulatory system was washed in isotonic saline and the animal finally transcardial perfusion fixed with 4% formalin and the brain was removed and postfixed in 4 % formalin for 24 hours.

2.6.3 Tissue Preparation

After 24 hours postfixation the 4% formalin was removed and the organs were washed three times in KPBS. Next organs were dehydrated in 30% sucrose for 24 hours after which the sucrose was removed and replaced with new 30% sucrose. Tissue specimens were then embedded in Tissue-Tek O.C.T (Sakura, 4583), mounted on specimen blocks, and frozen to optimal cutting temperature for each organ type. Finally the tissue specimens were cut into 30-35 µm serial coronal sections at -25-30°C on a cryostat, (Microm, HM 505N) and stored as free floating sections in KPBS with 0.02 % sodium azide as a preservative.

2.6.4 Immunohistochemistry

IHC was performed free-floating in Nunc™ containers.

Laminin immunohistochemistry was preformed with polyclonal rabbit anti-laminin as the primary antibody (DAKO, Z0097) diluted 1:100 in incubation buffer and incubated overnight at 4°C on a belly-dancer. Sections were washed three times in KPBS between each step. Next the sections were incubated with secondary antibodies for 1 hour at room temperature in incubation buffer containing 1:200 diluted goat-anti-rabbit Alexa 488 or Alexa Fluor 350 donkey anti-rabbit IgG. Finally the sections were transferred onto superfrost slides and allowed to air dry before being placed under coverslips with Pertex mounting media. Alexa Fluor 350 was used to stain laminin, when examining colocalization of OX26 stained with Alexa Flour 488 with OX26-MLs, as described below.

OX26 immunohistochemistry was performed on free floating brain sections from rats to detect previously injected OX26, which thus served as primary antibodies. Sections were incubated in incubation buffer containing 1:200 diluted donkey anti-mouse conjugated with Alexa Flour 555 overnight at 4°C on belly dancer. Alternatively tissue specimens containing MLs or OX26 MLs, sections were incubated in incubation buffer containing 1:200 diluted biotinylated rabbit anti-mouse antibodies (DAKO, E0464) overnight, followed by incubation for 1 hour at room temperature in PBS containing 1:200 streptavidin Alexa Flour 488 (Invitrogen, S32354). Alexa Flour 488 staining of OX26 was performed in order to study colocalization of OX26 with OX26-MLs in vivo, because Alexa Flour 555 overlaps with the particles emission spectrum.

2.7 Fluorescence Microscopy

Fluorescence microscopy was performed using an inverted microscope either Axiovert 200M or Axio Observer.Z1 from Zeiss and images were captured with AxioCam MRm, a highly sensitive monochrome camera using the imaging software Axiovision v. 4.8.2, which was also used for editing the captured images. Note images are acquired by a monochrome camera. Hence, all images are pseudocolored using original colours of the fluorophores except images displaying the biodistribution where cyan is used to represent DAPI-staining for enhanced visualization.

3. Results

3.1 Antibody Purification and Testing

3.1.1 Yield and Purity

During the elution of antibodies the elutant was collected in different fractions. From these fractions an elution diagram was created (Figure 9) (Microsoft Excel 2007).

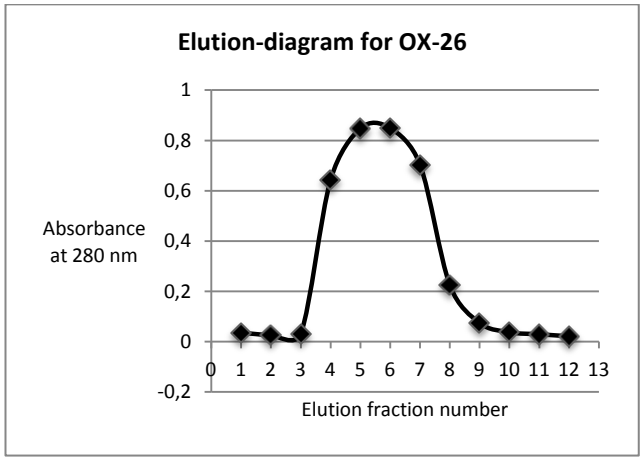

Figure 9: Elution diagram, X-axis shows the number of the elution fraction and Y-axis shows the absorbance at 280 nm.

Furthermore the purity was analyzed by running the different elution fractions on a 16 % SDS gel, which was stained with Coomasie stain (Figure 10). The lane marked 0, is a sample of the antibody:binding buffer suspension before it was run through the column showing a smear of proteins with many bands present on the gel indicating that the solution contained different serum and cellular proteins from the growth media and the hybridoma cell culture, respectively. Especially the 25 and 55 kDa bands stand out on the gel and correspond to the molecular weight of IgG light and heavy chains, respectively [Manjappa *et al.*, 2011]. Lane 1 is a sample taken from the flow-through when loading the antibody:binding buffer suspension onto column before elution of the antibodies, which shows a smear of proteins but almost a complete loss of protein bands at 25 and 55 kDa indicating that the complete IgG fraction had been absorbed on the column. The lane marked 2 contains a sample taken immediately before elution when running binding-buffer on the column in order to prepare for elution. A very slight protein band is seen at 25 and 55, which might indicate that the column had been slightly oversaturated with antibodies. Lanes 3-9 displays elution fractions 3-9, also seen in the elution diagram (Figure 9). The elution fractions clearly display the bands of 25 and 55 kDa and this demonstrates the specific elution of antibodies from the column with a high purity.

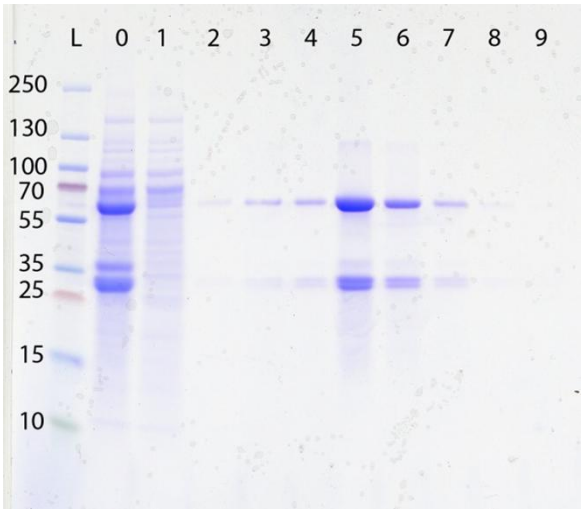

Figure 10: SDS gel stained with Coomasie Blue. L is the protein ladder (kDa), lane 0 is a sample of the antibody suspension before running on the column, lane 1 is a sample taken from the flow-through when loading the column with the antibody suspension and lane 2 is a sample of the flow-through just before beginning the elution of antibodies. Lane 3-9 is elution fractions 3-9 as seen in Figure 9. The gel clearly displays multiple protein bands on lane 0 and 1. However, the 25 and 55 kDa bands disappear in lane 1 indicating, that the antibodies were adsorbed to the column. A slight 25 and 55 kDa band in lane 2 indicate oversaturation of the column. Lanes 3-9 show pure elution fraction with only 25 and 55 kDa protein bands.

Elution fractions 4-7 were selected for purification by dialysis. After dialysis the antibody retrieval was 7.5 mL with 11.8 mg/ml, giving a total yield of 88.5 mg OX26 determined by the Bio-Rad RC DC Protein Assay as described in section 2.4.2 .

3.1.2 OX26 - RBE4 Binding Study

OX26 was tested against the anti-CD71 antibody in order to reveal if the staining pattern and binding were similar. Both antibodies performed excellent as primary antibodies with equivalent high fluorescence signals and stained both membrane bound as well as cytosolic transferrin receptors (Figure 11A, B, C, E, F and G). A slight unspecific staining is seen in the secondary control (Figure 11H), but very clearly different from the specific staining seen with primary antibodies added. This investigation demonstrated in vitro binding of OX26 and confirmed that the OX26-antibodies had not lost their affinity towards the transferrin receptor due to denaturation during the elution process.

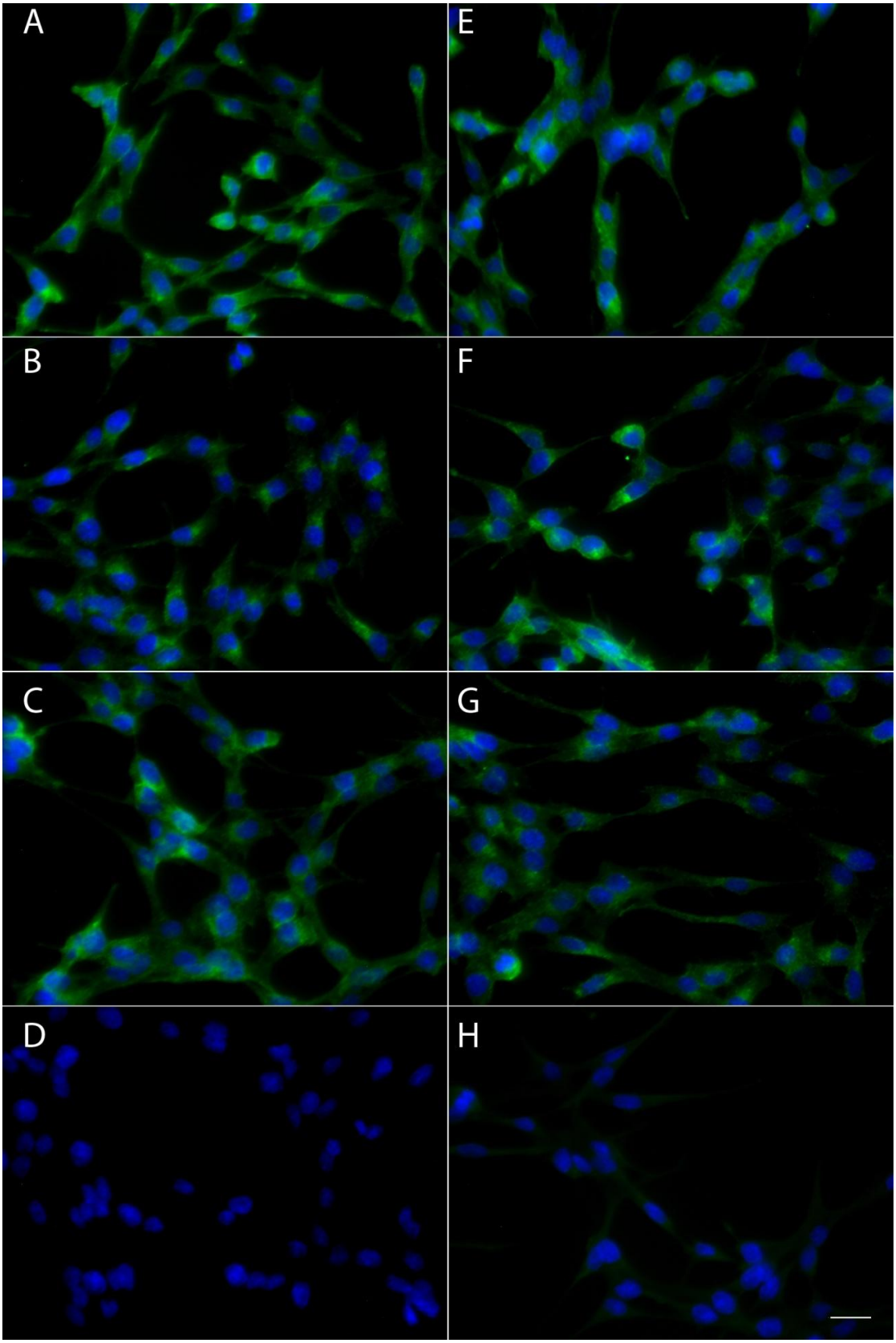

Figure 11: Merged images captured from RBE4 cells stained with either anti-CD71 (A, B & C) or OX26 (E, F and G) diluted 1:100, 1:200 and 1:400, respectively. Nuclei were counterstained with DAPI 2µg/ml. D represent DAPI staining of RBE4 cells, and H represent RBE4 cells stained without primary antibody with a slight autostaining. Images are captured at 400x magnification. Scale bar represents 20 µm.

3.1.3 OX26 - in vivo Binding Study

To determine the in vivo brain targeting potential of OX26 IHC was carried out on brain sections from a rat, which had previously been given an i.v. injection of 300 µg OX26 and on a control animal, which did not receive any OX26 (Figure 13). The staining pattern of OX26 in the brain sections indicate a clear and distinct labelling confined to the capillary bed. IHC was also performed to reveal the basal lamina by staining for laminin, but no staining of OX26 distal to laminin was found. The overlay images suggest a slight colocalization with laminin, which is displayed as yellow. However, no true colocalization analysis can be carried out, as the images were captured on a regular inverted fluorescence microscope and not on a confocal microscope.

3.2 Particle Characterization

The size of S-MNPs was determined to be 117.2 nm ± 1.17 nm with a PDI of 0.171 whereas the ζ-potential was -14.83 ± 0.42 mV. The size of MLs was determined to be 150.2 ± 2.44 nm with a PDI of 0.226 whereas the ζ-potential was 15.66 ± 1.65 mV. Finally the size of OX26 MLs was determined to be 181.9 ± 6.32 nm with a PDI of 0.298 and a ζ-potential of -7.14 ± 3.13 (Table 2).

	Size (nm)	PDI	Zeta potential (mV)
S-MNPs	117.2 ± 1.17	0.171	-14,83 ± 0.42
MLs	150.2 ± 2.44	0.226	15.66 ± 1.65
OX26-MLs	181.9 ± 6.32	0.298	-7.14 ± 3.13

Table 2: The size, PDI and Zeta potential of S-MNPs, MLs and OX26-MLs are displayed. Size and Zeta potential are given ± standard deviation.

The particle concentration in a typical batch of MLs and OX26-MLs was determined using the Prussian blue method and revealed a concentration of 1.37 ± 0.18 mg/ml and 1.30 mg/ml ± 0.17, respectively. The amount of antibody in the final OX26-ML batch was determined to be 0.54 mg/ml. This corresponds to ≈ 868 antibodies per OX26-ML (see 7.1). This calculation is based on the manufacturer's predicted particle number per gram $1.8x10^{15}$/g, the determined particle concentration and protein concentration in the final OX26-ML batch and furthermore it is assumed that the particles are aggregate free, all OX26 is associated with the particles, and the molecular weight of OX26 is 160,000 g/mol.

3.3 In Vitro Binding and Uptake Study

RBE4 cells were incubated for 3 hours with 1 µg S-MNPs, MLs or OX26-MLs (Figure 14). A low degree of uptake was observed with the unmodified S-MNPs; whereas both MLs and OX26-MLs showed improved binding and uptake by the RBE4 cells compared to S-MNPs. Interestingly MLs and OX26-MLs remained in the cytosol and a distinct perinuclear accumulation was noted. In order to provide a quantitative estimate of the particle uptake, each individual cell in the images was marked using a free hand selection tool. Next the mean fluorescence intensity for each cell was computed and the median fluorescence intensity for all cells was calculated and displayed in a bar plot (Figure 12).

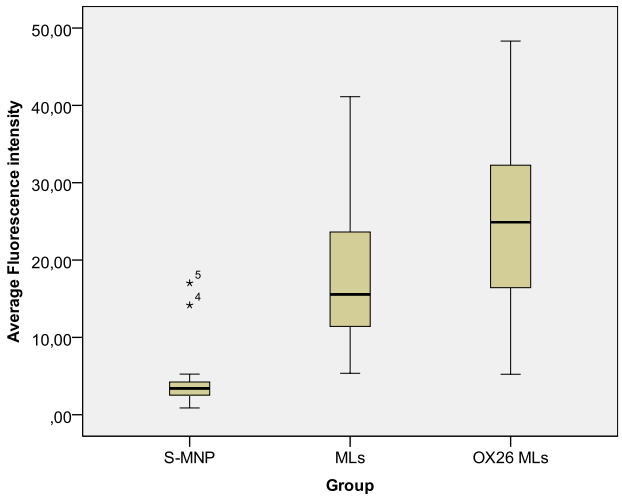

Figure 12: The bar plot boxes displays the 25-75% percentiles. Error bars represent the range of values from minimum to maximum. Stars indicate outliers. The median is displayed in each bar.

The median cell fluorescence intensity of MLs was increased 4.5 fold compared to S-MNPs, whereas OX26-MLs displayed a 7.3 fold and 1.6 fold increase in median cell fluorescence intensity compared to S-MNPs and MLs, respectively (Table 3).

	S-MNP	MLs	OX26-MLs
Median Fluorescence Intensity	3.4	15.6	24.9
Standard Deviation	3.7	9.3	11.5
Cell count	23	51	33

Table 3: The median cell fluorescence intensity, standard deviation and number of counted cells incubated with either 1 µg S-MNPs, MLs or OX26 MLs for 3 hours are displayed.

To determine, which groups were significant different from each other Mann-Whitney-U tests were run between the different groups. In summary both MLs and OX26-MLs have a median cell fluorescence intensity greater than S-MNPs and OX26-MLs had a significant greater median fluorescence intensity than MLs ($p < 0.05$).

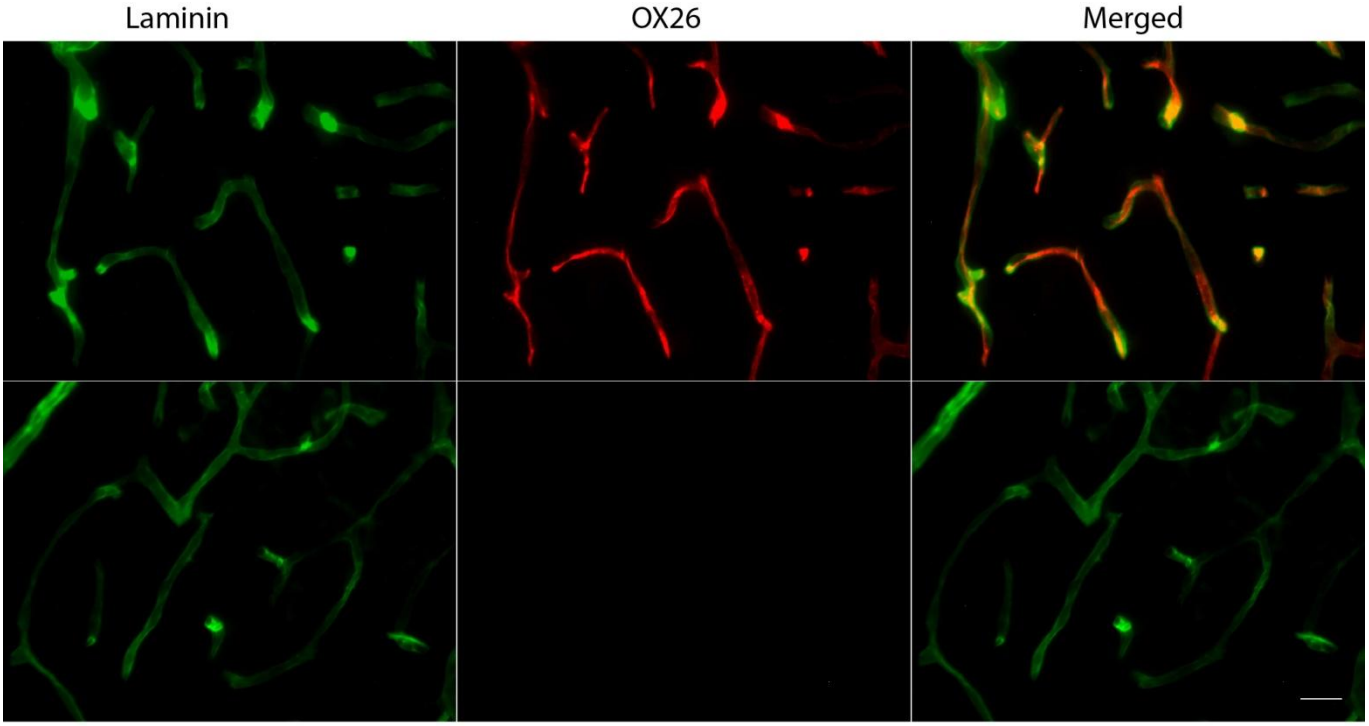

Figure 13: Upper row shows IHC staining for laminin (green) and OX26 (red) on brain sections from a rat administered i.v. with 300 µg OX26. The lower row shows IHC on rat brain sections from a control rat. Distinct labeling of the BCECs by OX26 is seen on brain sections from rats administered with OX26. All images are captured at 400x magnification and the scale bar represents 20 µm.

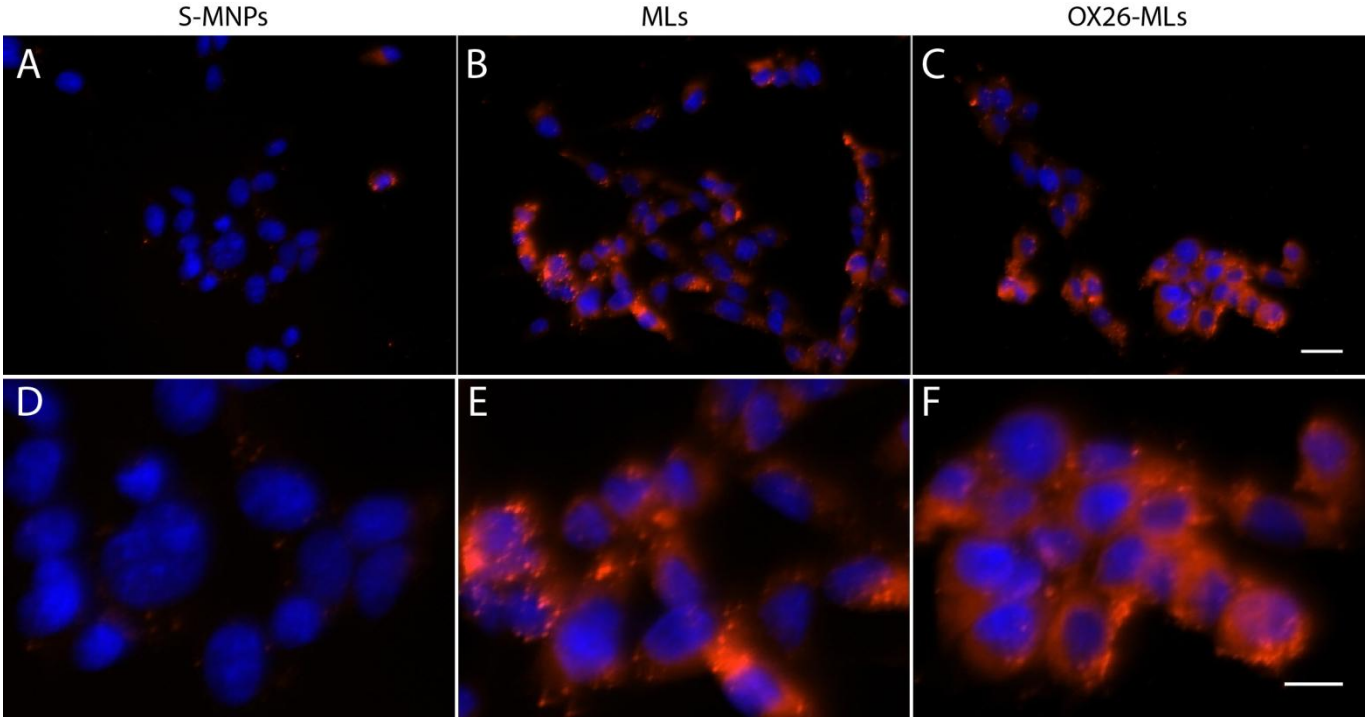

Figure 14: Represents merged images captured of DAPI-stained RBE4 cells cultured in a Permanox® chamber slides with 0.8 cm^2 per well. Each well was incubated with either 1 µg S-MNPs (A & D), MLs (B & E) or OX26 MLs (C & F). D, E and F represent cropped images of A, B and C, respectively. Images were captured at 400x magnification. The scale bar on C represents 20 µm and scale bar on F represents 10 µm.

3.4 Biodistribution Experiment

Following i.v. injection the main sites of accumulation for both MLs and OX26-MLs were the liver and spleen. The particles were also found to a much lesser extent in lung and in minute amounts in the kidney. The relative degree of accumulation in the spleen and liver between the MLs and OX26-MLs was difficult to judge; however, the MLs seem to be present in a somewhat higher degree in the spleen.

A distinct labelling pattern was observed for MLs in the liver, which appeared as labelling of small vessels by adsorption onto the vessel wall (Figure 16A& B). This phenomenon was not found for OX26-MLs (Figure 16D & E). In the lung both particle types displayed the same accumulation pattern localized to the septa of the alveoli (Figure 16C & F).

In the spleen both particles showed a distinct labelling pattern with a central zone of high cellular density, which was completely free of particles surrounded by a marginal zone with less cell density were the particles accumulated in a very high degree (Figure 17A, B, D & E). In the kidney it was difficult to find particles but occasionally a few of both particle types were found (Figure 17C& F).

Surprisingly, almost no brain accumulation of MLs and OX26-MLs were found since both type of particles were virtually absent in the brain capillaries. Occasionally a few OX26-MLs could be detected in the capillaries, but in very small amounts (Figure 15).

3.5 In situ Brain Perfusion Experiment

In situ perfusion experiments were performed on P16 rats, and the morphological distribution was investigated. The OX26 MLs showed pronounced labelling of the vascular bed in the brain (Figure 18). However, the labelling was not uniform but represented scattered particles present in the capillaries. No apparent difference in the degree of labelling of the capillary bed was found between brain sections from rats, which were exposed to a magnetic field and rats which were not. This indicated that the exposure to a magnetic field was not a necessary for OX26-MLs to be taken up by the BCECs. No labelling of the capillaries was found for MLs (data not shown but the captured images were the same, as when MLs were injected i.v. (Figure 15A)). After carefully examining several brain sections, from rats perfused with OX26-MLs and subjected to magnetic field exposure, some particles were found outside the vessel lumen in two sections indicating successful transcytosis of the OX26-MLs (Figure 19).

In order to demonstrate, that OX26 mediated the accumulation of OX26-MLs in the BCECs, IHC staining for OX26 was performed to demonstrate the localization of OX26 corresponding with the localization of OX26-MLs in the brain. The colocalization was evident although some OX26-staining was observed not associated with the OX26-MLs (Figure 20A, see arrows). This implies that the majority of OX26 remains associated with the OX26-MLs and mediate the binding and uptake in the BCECs.

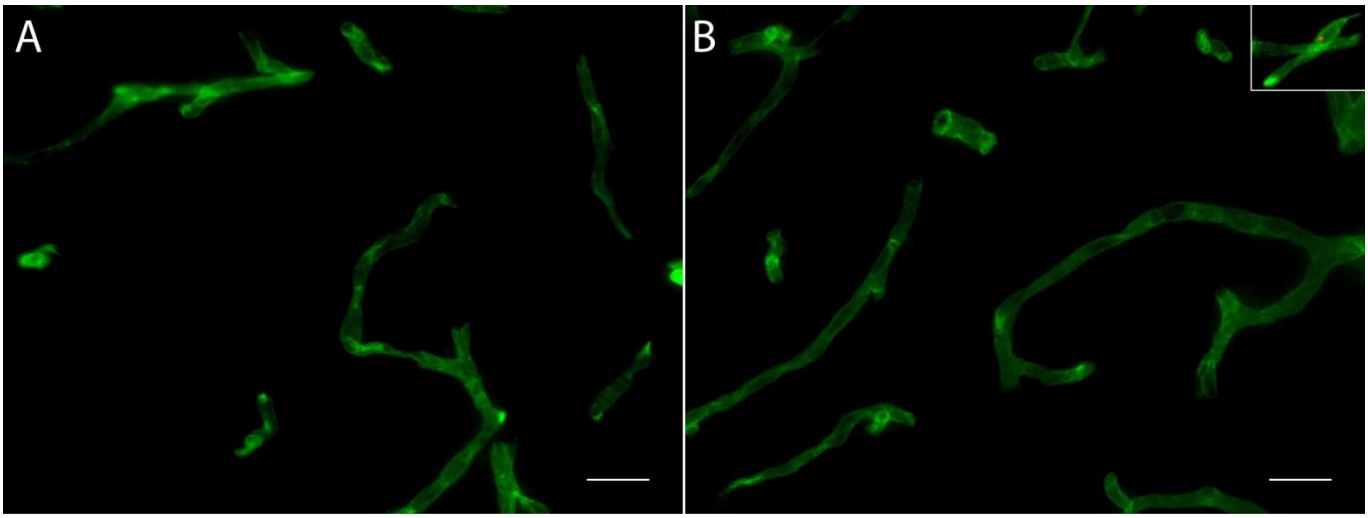

Figure 15: In vivo brain distribution of MLs and OX26-MLs. Images are from rats which received 10 µg/g bodyweight of MLs (A) or OX26-MLs (B), respectively by i.v. injection. An insert in the right corner, shows a single OX26-ML in a capillary. Both type of particles were virtually absent in the brain capillaries. Images are captured at 400x magnification and the scale bars represent 20 µm.

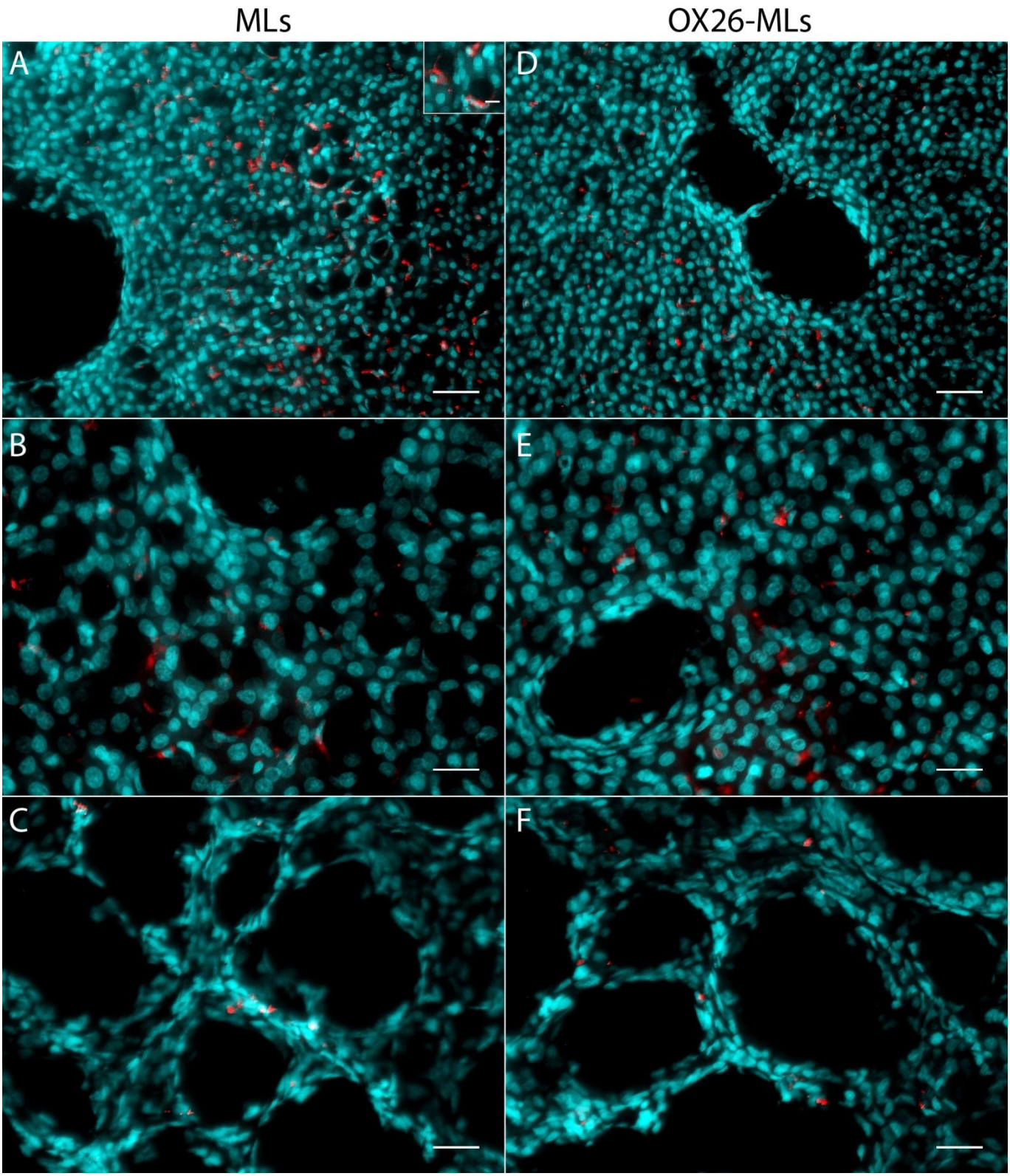

Figure 16: Biodistribution in the liver and lung. Image A and B show DAPI stained liver sections from a rat given MLs by i.v. injection. The insert in image A is a cropped and magnified part of the original image A, which shows a distinct labelling of the vessels lumen found exclusively in rats given MLs. Similar images (D & E) were captured from the liver of the rats given OX26-MLs; however, no labelling of the vessel lumen was found. C and F represent images of the lungs of rats given MLs and OX26-MLs respectively. Both particle types are found in the septa of the alveoli. Images B, C, E and F are captured at 400x magnification whereas A and D are captured at 200x magnification. Scale bars on 400x magnification images represent 20 µm, and scale bars on 200x images represent 40 µm. The insert's scale bar in picture A represents 10 µm.

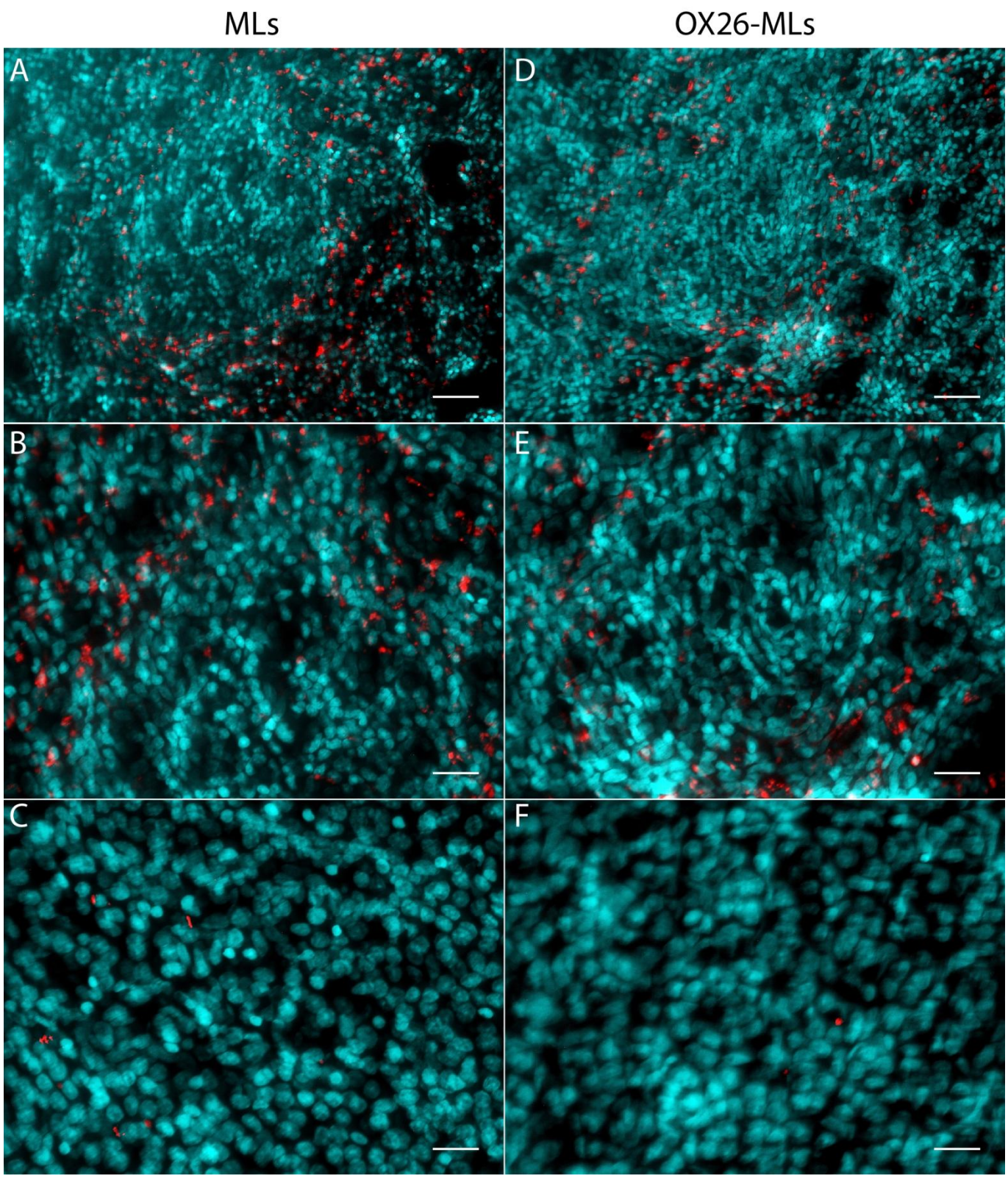

Figure 17: Biodistribution in the spleen and kidney. Images A and B shows DAPI-stained spleen sections from a rat given MLs. The images show a central zone with almost no particle accumulation, surrounded by a peripheral zone with a high degree of particle accumulation. Similar images were taken of spleen sections from a rat given OX26-MLs and the same pattern of particle accumulation was observed (D & E). Images C and F represent kidney sections, where very few particles could be found. Images B, C, E and F are captured at 400x magnification, whereas A and D are captured at 200x magnification. Scale bars on 400x magnification images represent 20 µm, and scale bars on 200x images represent 40 µm.

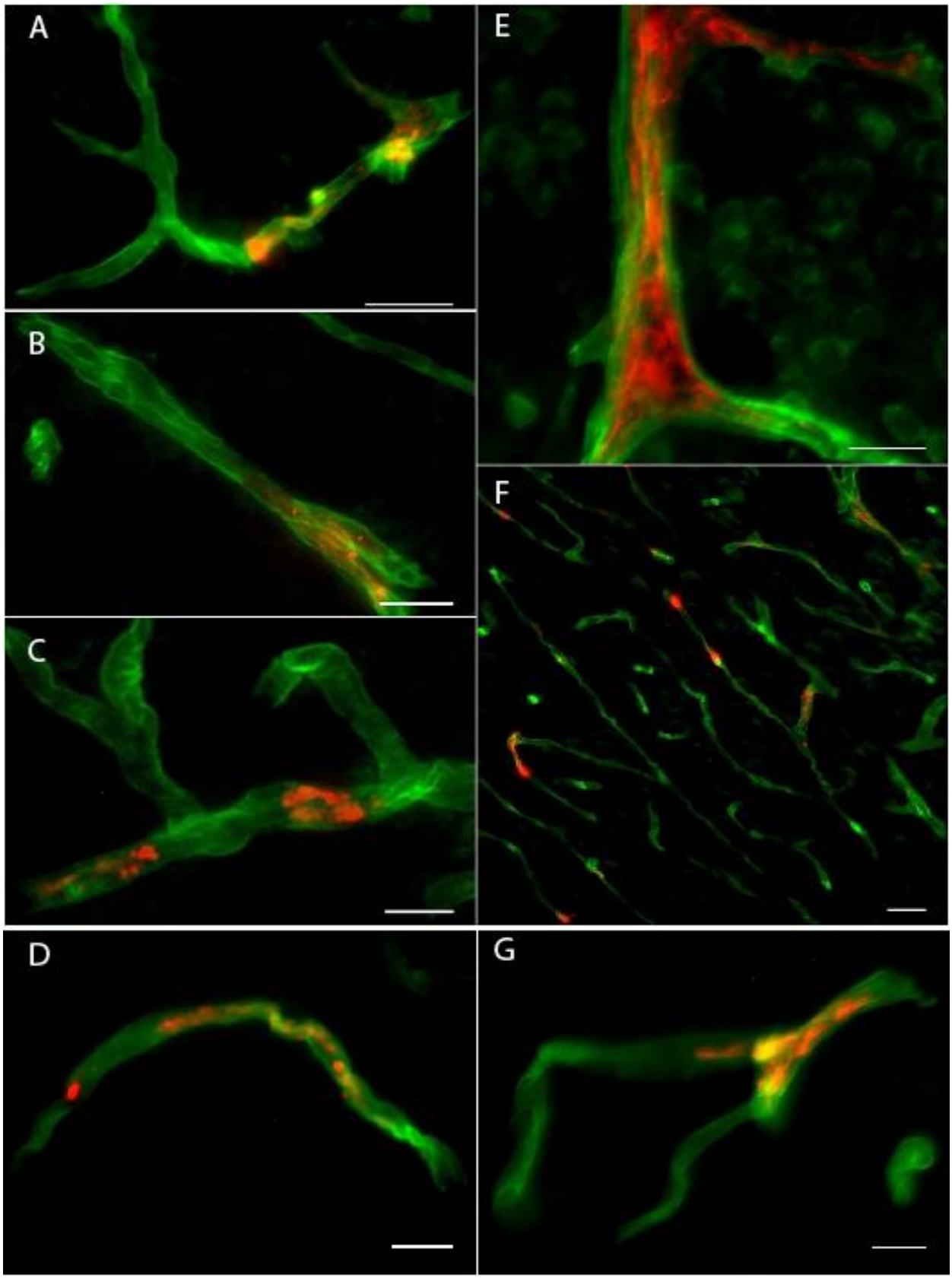

Figure 18: Merged images showing OX26-MLs and laminin IHC staining on rat brain sections. A, B, C, E and F are images captured of brain sections from rats, which were perfused with OX26-MLs and exposed to a magnetic field, showing particles in vessel lumen. E displays a larger vessel with several branches filled with particles. F represents a low magnification overview image of the capillary bed. D and G are both images captured of brain sections from rats, which were perfused with OX26-MLs but not exposed to a magnetic field. All images are cropped and all images except F are captured at 400x magnification. F is captured on 200x magnification. Scale bars on B, D and G represent 10 µm and scale bars on A, C and F represent 20 µm.

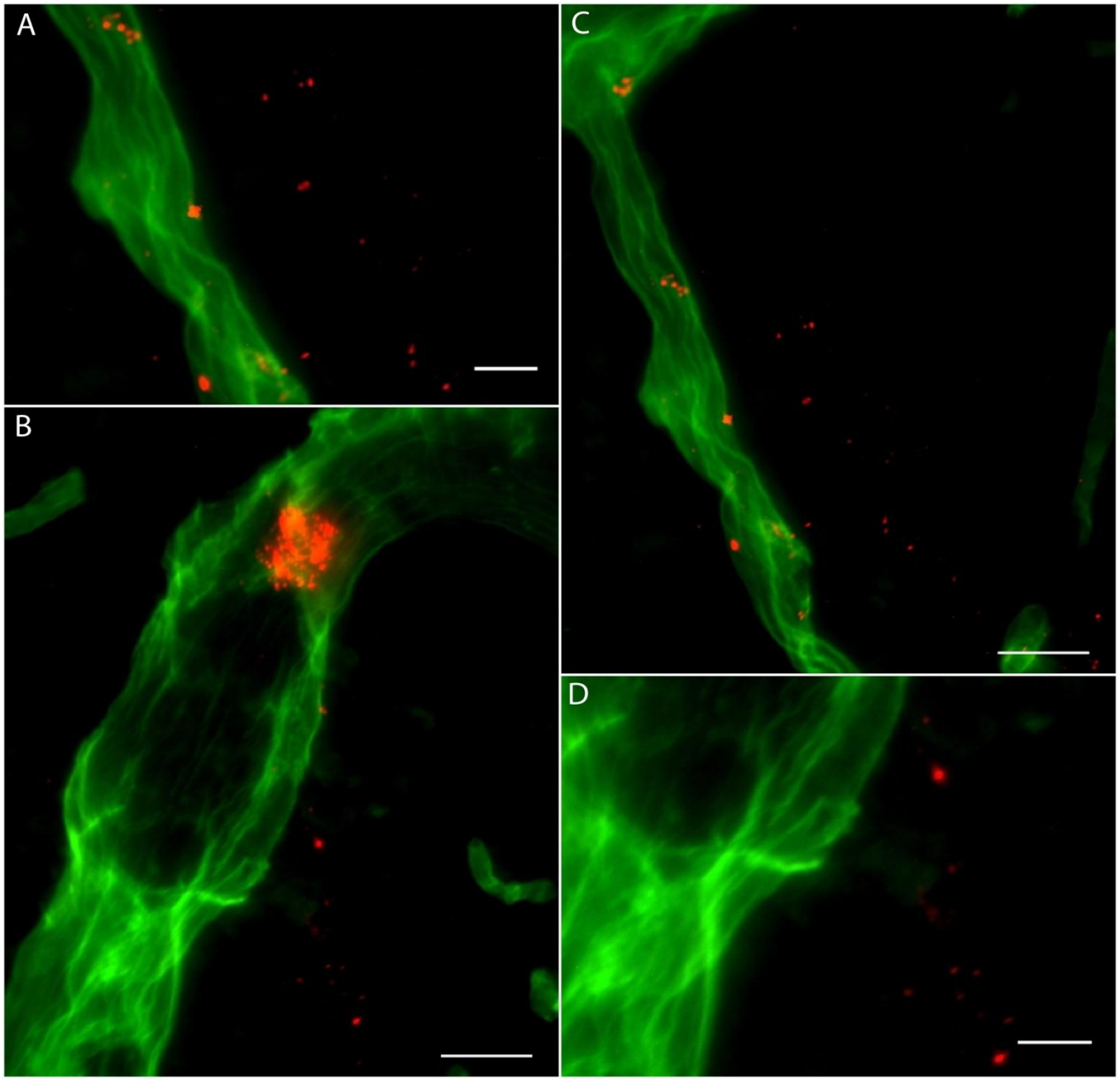

Figure 19: Merged images display IHC staining of laminin on brain tissue sections from rats, which were perfused with OX26-MLs and exposed to a magnetic field. OX26-MLs are seen in the lumen of the vessels. However, more interestingly OX26-MLs were also found beyond the abluminal side of the vessels. All images are cropped. A is a magnified part of C while D is a magnified part of B. Images are captured on 400x magnification. Scale bars on image A & D represent 10 µm while scale bars on B & C represent 20 µm.

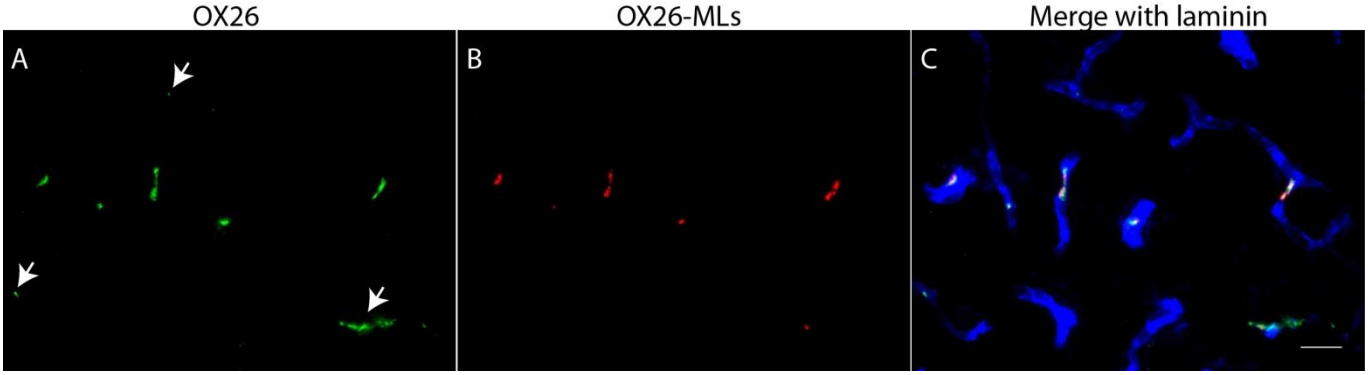

Figure 20: Colocalization of OX26 with OX26-MLs. A represents OX26 IHC staining, B represents OX26-MLs, and C is a merged image of A and B with laminin. Arrows indicate OX26 staining with no colocalization with OX26-MLs. Images are captured at 400x magnification and the scale bar represents 20 µm.

4. Discussion

4.1 Methodological Considerations on the situ Brain Perfusion Technique

In situ brain perfusion was used in the present study to demonstrate accumulation of OX26-MLs and MLs in the BCECs. P16 rats were used due to their high expression and recycling rate of transferrin receptors by the BCECs and their small systemic blood volume [Moos & Morgan, 2002; Morgan & Moos, 2002]. These features make P16 rats an ideal model for studying OX26 mediated delivery and in situ transcardial perfusion feasible without the risk of hypoperfusion with consequent ischemia. The in situ perfusion method has the major advantage of allowing complete control over the perfusion fluid constituents and the concentration of the test compound. This eliminates the risk of degradation or aggregation after administration by plasma components, which can occur after i.v. administration. The method also suffers from some drawback for example the perfusion period is limited to 15 minutes as longer perfusion periods can cause hypoxia at the BBB and consequently compromising the integrity, which will obscure the experiments [Roberts *et al.*, 1993]. Furthermore the perfusion time limits the experiment to study processes which occurs within the 15 minute time frame. This should not constitute a problem for studying OX26 mediated transport, as the same time frame or shorter have previously been used [Gosk *et al.*, 2004; Cerletti *et al.*, 2000; Bickel *et al.*, 1994].

4.2 Particle Characteristics

The successful preparation of MLs was confirmed by an increase in particle size of S-MNPs from 117.2 nm ± 1.17 to 150.2 ± 2.44 for MLs. Furthermore, this increase in size was accompanied by an increase in the zeta potential from -14.83 ± 0.42 to +15.66 ± 1.65, which strongly indicates encapsulation in a cationic lipid layer. Since a single phospholipid bilayer has a thickness of 5 nm and the corona formed by PEG-2000 also has a thickness of 5 nm an apparent increase of 20 nm in total diameter would be expected [Schnyder & Huwyler, 2005]. However, the increase is an additional 10 nm, which suggests the lipid encapsulation entraps a volume of water along with the particles. In addition the PDI increases from 0.171 to 0.226 indicating a more inhomogeneous sample presumable due to encapsulation of S-MNPs in liposomes of diverse sizes.

After conjugating OX26 to MLs the particle size increased to 181.9 ± 6.32, which is an increase of roughly 30 nm. This size gain corresponds with conjugation of the antibodies to the surface of the lipid wall, since the length of antibodies are 15 nm [Schnyder & Huwyler, 2005]. The increase in PDI to 0.298 indicates a low level of aggregates formed during the antibody transfer from micelles to MLs, since the temperature during this step is above the phase transition temperature, which allows lipid membranes to fuse. The zeta potential of the OX26-MLs was reduced by approximately 20 mV, which is probably a result of the transfer of anionic DSPE-PEG2000-maleimide from the micelles to the MLs. Incorporation of anionic PEGylated phospholipids have previously been reported to reduce the zeta potential of cationic magnetoliposomes by roughly 20 mV [Dandamudi & Campbell, 2007].

The cellular uptake of particles has previously been shown to depend on a homogenous size distribution. Furthermore, the size of the particles is vital to avoid occlusion of capillaries. It has previously been proposed, that an acceptable PDI is < 0.3 and particles should not be larger than 1.4 µm to avoid formation of emboli and allow uniform tissue perfusion [Senyei *et al.*, 1978; Zhang *et al.*, 2010]. Hence, the particles used in this study meet these criteria with a mean size lower than 200 nm for all particles, and a PDI within an acceptable range (< 0.3).

In the present study the antibody density was estimated to be 868 per OX26-ML. This is a very high antibody density, which can prove counterproductive as less may prove to be more. Indeed it has previously been shown for 100 nm OX26-PILs, that antibody densities above 30 reduce the in vivo binding to BCECs drastically [Huwyler *et al.*, 1996]. In addition, using a antibody density of 29 it was demonstrated, that the systemic clearance increased 5-fold compared to non-targeted PILs [Huwyler *et al.*, 1996]. Hence, it can be speculated if particles with a much higher antibody density as used in the present study have a significantly higher clearance and if this can account for reduced uptake efficiency by BCECs in the present study. However, this is probably not the case as a comparison between the clearance of OX26-PILs with antibody densities of 29 and 197, respectively, revealed an approximately 30 % lower clearance for OX26-PILs with a antibody density of 197 [Huwyler *et al.*, 1996]. The injected dose found in the brain was nevertheless more than 3-fold increased for OX26-PILs with an antibody density of 29. Therefore, it can be assumed, that the high antibody density interferes with the binding of OX26-PILs to the

BCECs, which can also have negatively affected the uptake of OX26-MLs by the BCECs in the present study.

4.3 In vitro Cellular Uptake of Particles

The initial in vitro uptake study demonstrated the effect of encapsulating S-MNPs in a cationic lipid layer. The cellular uptake was increased dramatically demonstrated by a 4.5 fold increase in the median fluorescence intensity. This finding is supported by a previously reported high uptake of cationic liposomes in microvascular endothelial cells [Dandamudi & Campbell, 2007]. Furthermore, the perinuclear accumulation was also noted by Dandamudi and colleges, which seems to be a specific accumulation pattern for endothelial cells. The uptake of OX26-MLs increased even further when OX26 was conjugated to the MLs demonstrated by a 7.3 fold increase compared to S-MNPs and a 1.6 fold increase compared to MLs.

This striking difference of cellular uptake in RBE4 cells proves that the synthesis of MLs and OX26-MLs was successful. The increased uptake of MLs compared to S-MNPs is probably due to the favourable interaction of cationic liposomes with the cell membrane and uptake mediated by adsorptive endocytosis, whereas the increased uptake of OX26 are due to receptor-mediated endocytosis. The specific uptake mechanisms could be further elucidated by using specific inhibitors of endocytosis [Ivanov, 2008].

In addition the extensive uptake of both particles in RBE4 cells highlights the potential usage of MLs as well as OX26-MLs for in vivo imagining and cell tracking, as these superparamagnetic nanocarriers are suitable for MRI. MNPs with a high accumulation in cells have already proven useful in cell tracking in stem cell research [Cromer Berman *et al.*, 2011]. For this to be viable for MLs and OX26-MLs synthesized in the present study, it remains to be demonstrated, that these particles possess a low toxicity, a high intracellular stability and do not interfere with normal cellular functions.

4.4 Morphological Distribution of OX26 in the Brain

The initial study on RBE4 cells demonstrated the affinity of the purified OX26 antibodies to the transferrin receptor. This was furthermore examined by i.v injection of OX26 in rats. The results clearly demonstrated a distinct labelling of the capillaries consistent with targeting and uptake into the BCECs. The images acquired by fluorescence microscopy suggested that OX26 reached the basement membrane, but not a single indication of OX26 beyond the basement membrane was found. The labelling of the BCECs are consistent with previous research investigating the immunohistochemical distribution of OX26 in the brain [Gosk *et al.*, 2004; Moos & Morgan, 2001; Pardridge *et al.*, 1991; Friden *et al.*, 1991]. However the labelling of the basement membrane is not a consistent finding. Paris-Robidas and colleges who have previously investigated the anti-mouse anti-transferrin receptor antibody analogue to OX26 reported a slight co-localization with the basement membrane but found no evidence of passage beyond this [Paris-Robidas *et al.*, 2011]. However, Gosk et al. found no apparent transcytosis and colocalization with the basal membrane [Gosk *et al.*, 2004]. The fluorescence images acquired in this study cannot be used for true colocalization analysis as multiple planes are excited when using fluorescence microscopy. Confocal microscopy will therefore have to determine if OX26 colocalizes with the basement membrane and to which extent this occurs.

The results obtained in this study demonstrated, that OX26 was confined to the BCECs. These results are contrary to what other researchers have reported by using indirect outcome measures. As mentioned in section 1.3.1 OX26 has been utilized as a standalone drug delivery system by conjugating a diversity of therapeutics directly to OX26 or via the biotin/avidin technology. OX26 conjugated to epidermal growth factor, basic fibroblast growth factor or VIPa has been used to image C6 glioblastoma [Kurihara & Pardridge, 1999], induce neuroprotection after an ischemic event [Song *et al.*, 2002; Wu & Pardridge, 1999] and to cause cerebral vasodilatation [Bickel *et al.*, 1993], respectively. However, both brain cancer as well as ischemic insults are known to induce a compromised BBB [Plateel *et al.*, 1997; Wolburg *et al.*, 2003], which facilitate passive permeation across the BBB were the effect can be exerted, and the increased vasodilation caused by OX26 conjugated to VIPa may be a result of increased delivery to the BCECs. Other researcher have investigated the passage of OX26 without therapeutic compounds by direct evidence including Bickel et al. who demonstrated gold conjugated OX26 at the luminal membrane, in the cytoplasm, and even at the abluminal membrane of BCECs [Bickel *et al.*, 1994]. However Bickel et al. did not find any gold-conjugates in the parenchyma, although they did suggest exocytosis of OX26 [Bickel *et al.*, 1994]. Moos & Morgan also investigated the distribution of OX26 and found no evidence of transcytosis [Moos & Morgan, 2001]. To summarize no immunohistochemical

evidence has been provided to show that OX26 is delivered across a functional intact BBB. The studies using disease models to demonstrate the brain targeting capacity of OX26 lack awareness of the disease models effect on the BBB, which leads to erroneous conclusions.

4.5 Morphological Biodistribution

The biodistribution of both particles displayed an expected distribution pattern with a preferential accumulation in the spleen and liver and a minor accumulation in the lung and kidney (Figure 16 & Figure 17).

Both particles showed a distinct labelling pattern in the spleen with a central zone of high cellular density, which were almost completely free of particles surrounded by a zone with less cell density were the particles accumulated in a high degree (Figure 17A, B, D & E). The central zone could correspond to the white pulp, whereas the zone which borders the white pulp could be the marginal zone. The marginal zone is specialized in trapping particulate antigens from the circulation for further processing and recognition [Kraal, 1992]. However, only substances that are immunogenic are trafficked to the white pulp. The high degree of accumulation seen in the marginal zone is probably due to marginal zone macrophages, which show excellent phagocytotic capabilities [Kraal, 1992].

The large uptake in the liver is most likely associated with the presence of Kupffer cells. Furthermore, a higher accumulation in the liver would be expected for OX26-MLs than for MLs, since this has previously been reported due to the fact that the Kupffer cells express Fc-receptors [Aragnol & Leserman, 1986] and hepatocytes express transferrin receptors on their membrane [Crichton *et al.*, 2002]. Nevertheless, the uptake by the liver parenchyma may be limited due to relatively large size of both MLs and OX26-MLs, which is 150 and 180, respectively, while the fenestrations of the sinusoids have been reported to be within the range of 50-170 nm [Cogger & Le Couteur, 2009; Cogger *et al.*, 2010]. The Kupffer cells line the liver sinusoids and therefore the particles can avidly be taken up by these cells [Wisse *et al.*, 1996]. The apparent labelling of the vessels' lumen, seen in liver sections from rats given MLs i.v., could thus represent liver sinusoids with Kupffer cells having phagocytosed the particles (Figure 16A & B). However, the size of the labelled vessels may be too large to represent sinusoids, which have a diameter of 5-8 µm. Alternatively, the vessels can represent arterioles, capillaries or small veins. The reason for the vascular labelling can be related to the zeta potential of the MLs, which will cause a favourable interaction with the endothelial cells, whereas this is not observed for OX26-MLs probably due to their reduced zeta potential.

The apparent lack of accumulation of MLs in the brain capillaries was expected; however, the absence of OX26-MLs was surprising (Figure 15). The reason for this phenomenon may be loss of colloid stability and aggregation of the OX26-MLs, when injected i.v., which have previously been described for starch coated MNPs [Alexiou *et al.*, 2006]. Another explanation could be adsorption of serum proteins unto the OX26-MLs, which could both facilitate loss of colloidal stability and inhibit the interaction of the OX26 antibodies with the transferrin receptors.

However, a lack of colloid stability and consequently aggregation would be expected to cause a higher degree of accumulation in the first-pass capillary bed, namely in the lung, which have previously been described for cationic liposomes as well as PEGylated cationic liposomes [Hong *et al.*, 1997]. Yet, only a relatively small amount of particles were accumulated in the lung for both particle types, but it is plausible, that the aggregates formed are still small enough to uniformly perfuse the capillary bed of the lung and avoid accumulation.

4.6 Morphological Distribution of OX26-MLs in the Brain

After 15 minutes transcardial in situ brain perfusion only OX26-MLs were localized to the BCECs whereas MLs were absent (Figure 18). This demonstrates that the successful targeting of OX26-MLs to the BCECs is mediated by OX26. Furthermore carefully examining several brain sections revealed no OX26-MLs in the brain parenchyma for rats in situ perfused with OX26-MLs but not exposed to a magnet. However, some OX26-MLs were found outside the vessels in a few instances in brain sections from rats subjected to magnetic field exposure during the in situ brain perfusion (Figure 19). Whether this phenomenon represents true transcytosis of OX26-MLs or is due to a compromised BBB or an artefact from handling and tissue preparation remains unknown.

Another important aspect was to clarify if OX26 mediated the enhanced uptake of OX26-MLs. Therefore, the colocalization of OX26 with OX26-MLs was examined and was found to colocalize. This provides proof that OX26 remains associated with OX26-MLs and mediates the binding of the OX26-MLs to the BCECs. However, some OX26 did not colocalize with the particles (Figure 20 A, see ar-

rows), which indicates that a fraction of the OX26 was unbound, and as a result further purification may be need of the OX26-MLs before usage to remove all unbound OX26. In addition this will reduce the predicted antibody density but to which extent remains unclear.

The results obtained in this study cannot be directly compared to other studies, as this is the first study to utilize OX26-MLs for drug delivery to the brain. However this drug delivery system is similar to OX26-PILs, which will therefore be the frame of reference. The results obtained in the present study do not correlate with previously research, which have reported that OX26-PILs can be delivered to the brain parenchym [Huwyler *et al.*, 1996; Cerletti *et al.*, 2000; Shi *et al.*, 2001; Shi & Pardridge, 2000; Zhang *et al.*, 2003a]. Huwyler et al. showed that OX26-PILs loaded with H^3-radiolabeled daunomycin accumulated in the brain in a higher degree than free H^3-radiolabeled daunomycin. However, the measurements were done on whole brain homogenates and only daunomycin was labelled not the liposomes or OX26. These facts make it impossible to exclude the accumulation occurred at the BCECs and impossible to comment on the accumulation of liposomes and OX26. Another study performed by Cerletti and colleges used in situ perfusion for 7 min followed by capillary depletion technique and found OX26-PILs in the brain parenchyma. However, no quality control was performed to confirm the successful separation of the vascular fraction from the brain fraction and no data was given for the vascular fraction.

Pardridge and colleagues have demonstrated that OX26-PILs loaded with short hairpin RNA for the luciferase gene were able to cause gene-silencing in C6 rat glioblastoma cells permanently transfected with luciferase gene [Zhang *et al.*, 2003a]. However, it is well known that glioblastoma models exhibit an impaired BBB [Wolburg *et al.*, 2003]. In addition Pardridge and colleagues concluded that OX26-PILs containing β-galactosidase plasmids were able transfect neurons, glia cells and endothelial cells after i.v. injection [Shi & Pardridge, 2000; Shi *et al.*, 2001]. However, it is impossible to conclude which cell types were actually transfected as only low magnification images of whole brain sections were presented [Shi & Pardridge, 2000]. A general problem with the above studies is the use of indirect outcome measures in disease models, which are not suitable to demonstrate transport across the BBB.

To summarize no conclusive evidence supporting the notion of transcytosis of the OX26-PILs across an uncompromised BBB has been provided by previous research. The localization of the OX26-MLs are in good concordance with Gosk et al., who were unsuccessful in demonstrating OX26-PILs in the post vascular compartment by both IHC and capillary depletion technique but demonstrated profound accumulation in the BCECs [Gosk *et al.*, 2004].

Unfortunately, the experimental evidence for blood to brain delivery of OX26-ML provided by this study is very limited. However, blood to endothelium transport seems to be feasible with OX26-MLs. Previously studies utilizing hemagglutination virus of Japan-liposomes loaded with GDNF plasmids have demonstrated transfection of BCECs after i.v. injection and furthermore GDNF was found to be secreted abluminal into the brain parenchyma [Jiang *et al.*, 2002; Jiang *et al.*, 2003]. This provides a promising usage of the OX26-MLs to mediate transfection of BCEC in order to facilitate secretion of functional neurotherapeutic proteins for the treatment of brain disorders. The author has previously demonstrated transfection of RBE4 cells in vitro with cationic MLs suggesting that this can also be feasible with OX26-MLs.

5. Conclusion

The overall goal of this thesis was to develop a novel magnetic responsive drug delivery system to enable transport across the BBB. For this purpose OX26-MLs were successfully prepared and demonstrated enhanced uptake in RBE4 cells in vitro. In vivo biodistribution experiments did reveal a similar biodistribution for OX26-MLs and MLs. Surprisingly, no significant accumulation of OX26-MLs were seen in the brain capillaries. This might be explained by a lack of colloidal stability of OX26-MLs in full blood, which could interfere with the binding to the BCECs and consequently the uptake. Therefore the stability in blood must be improved to allow i.v. administration. In situ perfusion experiments revealed that OX26-MLs demonstrate good potential as a drug delivery system to the BCECs with enhanced uptake compared to MLs. Furthermore, the uptake did not seem to be depended on an external magnetic field and hence OX26-MLs are probably transported into the BCECs by receptor mediated endocytosis. When investigating the permeation of OX26-MLs under the influence of a magnetic field a small amount of OX26-MLs were found beyond the BBB, which suggests transcytosis occurred; however, no convincing and consistent evidence was found for this phenomenon to support widespread transcytosis and cellular accumulation of OX26-MLs beyond the BBB.

6. References

Abbott N.J. (2002) Astrocyte–endothelial interactions and blood–brain barrier permeability*. *Journal of Anatomy,* **200,** 629-638.

Abbott N.J., Patabendige A.A., Dolman D.E., Yusof S.R. & Begley D.J. (2010) Structure and function of the blood-brain barrier. *Neurobiol Dis,* **37,** 13-25.

Alam M.I., Beg S., Samad A., Baboota S., Kohli K., Ali J., Ahuja A. & Akbar M. (2010) Strategy for effective brain drug delivery. *European Journal of Pharmaceutical Sciences,* **40,** 385-403.

Alexiou C., Arnold W., Klein R.J., Parak F.G., Hulin P., Bergemann C., Erhardt W., Wagenpfeil S. & Lubbe A.S. (2000) Locoregional cancer treatment with magnetic drug targeting. *Cancer Res,* **60,** 6641-8.

Alexiou C., Jurgons R., Schmid R.J., Bergemann C., Henke J., Erhardt W., Huenges E. & Parak F. (2003) Magnetic drug targeting--biodistribution of the magnetic carrier and the chemotherapeutic agent mitoxantrone after locoregional cancer treatment. *J Drug Target,* **11,** 139-49.

Alexiou C., Jurgons R., Seliger C. & Iro H. (2006) Medical applications of magnetic nanoparticles. *J Nanosci Nanotechnol,* **6,** 2762-8.

Allen T.M. (1994) Long-circulating (sterically stabilized) liposomes for targeted drug delivery. *Trends Pharmacol Sci,* **15,** 215-20.

Allt G. & Lawrenson J.G. (2001) Pericytes: cell biology and pathology. *Cells Tissues Organs,* **169,** 1-11.

Aragnol D. & Leserman L.D. (1986) Immune clearance of liposomes inhibited by an anti-Fc receptor antibody in vivo. *Proc Natl Acad Sci U S A,* **83,** 2699-703.

Astradsson A., Jenkins B.G., Choi J.-K., Hallett P.J., Levesque M.A., Mcdowell J.S., Brownell A.-L., Spealman R.D. & Isacson O. (2009) The blood–brain barrier is intact after levodopa-induced dyskinesias in parkinsonian primates—Evidence from in vivo neuroimaging studies. *Neurobiology of Disease,* **35,** 348-351.

Bagley R.G., Weber W., Rouleau C. & Teicher B.A. (2005) Pericytes and endothelial precursor cells: cellular interactions and contributions to malignancy. *Cancer Res,* **65,** 9741-50.

Bali P.K., Zak O. & Aisen P. (1991) A new role for the transferrin receptor in the release of iron from transferrin. *Biochemistry,* **30,** 324-328.

Beduneau A., Hindre F., Clavreul A., Leroux J.C., Saulnier P. & Benoit J.P. (2008) Brain targeting using novel lipid nanovectors. *J Control Release,* **126,** 44-9.

Bickel U., Kang Y.S., Yoshikawa T. & Pardridge W.M. (1994) In vivo demonstration of subcellular localization of anti-transferrin receptor monoclonal antibody-colloidal gold conjugate in brain capillary endothelium. *J Histochem Cytochem,* **42,** 1493-7.

Bickel U., Yoshikawa T., Landaw E.M., Faull K.F. & Pardridge W.M. (1993) Pharmacologic effects in vivo in brain by vector-mediated peptide drug delivery. *Proc Natl Acad Sci U S A,* **90,** 2618-22.

Bickel U., Yoshikawa T. & Pardridge W.M. (2001) Delivery of peptides and proteins through the blood–brain barrier. *Advanced Drug Delivery Reviews,* **46,** 247-279.

Boutry S., Forge D., Burtea C., Mahieu I., Murariu O., Laurent S., Vander Elst L. & Muller R.N. (2009) How to quantify iron in an aqueous or biological matrix: a technical note. *Contrast Media Mol Imaging,* **4,** 299-304.

Cardoso F.L., Brites D. & Brito M.A. (2010) Looking at the blood–brain barrier: Molecular anatomy and possible investigation approaches. *Brain Research Reviews,* **64,** 328-363.

Carvey P.M., Zhao C.H., Hendey B., Lum H., Trachtenberg J., Desai B.S., Snyder J., Zhu Y.G. & Ling Z.D. (2005) 6-Hydroxydopamine-induced alterations in blood–brain barrier permeability. *European Journal of Neuroscience,* **22,** 1158-1168.

Cerletti A., Drewe J., Fricker G., Eberle A. & Huwyler J. (2000) Endocytosis and Transcytosis of an Immunoliposome-Based Brain Drug Delivery System. *Journal of Drug Targeting,* **8,** 435-446.

Chertok B., David A.E., Moffat B.A. & Yang V.C. (2009) Substantiating in vivo magnetic brain tumor targeting of cationic iron oxide nanocarriers via adsorptive surface masking. *Biomaterials,* **30,** 6780-6787.

Chertok B., David A.E. & Yang V.C. (2010) Polyethyleneimine-modified iron oxide nanoparticles for brain tumor drug delivery using magnetic targeting and intra-carotid administration. *Biomaterials,* **31,** 6317-6324.

Cogger V.C. & Le Couteur D.G. (2009) Fenestrations in the Liver Sinusoidal Endothelial Cell. *The Liver.* John Wiley & Sons, Ltd.

Cogger V.C., Mcnerney G.P., Nyunt T., Deleve L.D., Mccourt P., Smedsrød B., Le Couteur D.G. & Huser T.R. (2010) Three-dimensional structured illumination microscopy of liver sinusoidal endothelial cell fenestrations. *Journal of Structural Biology,* **171,** 382-388.

Crichton R.R., Wilmet S., Legssyer R. & Ward R.J. (2002) Molecular and cellular mechanisms of iron homeostasis and toxicity in mammalian cells. *J Inorg Biochem,* **91,** 9-18.

Cromer Berman S.M., Walczak P. & Bulte J.W.M. (2011) Tracking stem cells using magnetic nanoparticles. *Wiley Interdisciplinary Reviews: Nanomedicine and Nanobiotechnology,* **3,** 343-355.

Crowe A. & Morgan E.H. (1992) Iron and transferrin uptake by brain and cerebrospinal fluid in the rat. *Brain Res,* **592,** 8-16.

Dallas S., Miller D.S. & Bendayan R. (2006) Multidrug resistance-associated proteins: expression and function in the central nervous system. *Pharmacol Rev,* **58,** 140-61.

Dandamudi S. & Campbell R.B. (2007) Development and characterization of magnetic cationic liposomes for targeting tumor microvasculature. *Biochimica et Biophysica Acta (BBA) - Biomembranes,* **1768,** 427-438.

Dautry-Varsat A., Ciechanover A. & Lodish H.F. (1983) pH and the recycling of transferrin during receptor-mediated endocytosis. *Proc Natl Acad Sci U S A,* **80,** 2258-62.

Demeule M., Poirier J., Jodoin J.*, et al.* (2002) High transcytosis of melanotransferrin (P97) across the blood–brain barrier. *Journal of Neurochemistry,* **83,** 924-933.

Dogrukol-Ak D., Banks W.A., Tuncel N. & Tuncel M. (2003) Passage of vasoactive intestinal peptide across the blood–brain barrier. *Peptides,* **24,** 437-444.

Dohrmann G.J. (1970) The choroid plexus: A historical review. *Brain Research,* **18,** 197-218.

Forbes Z.G., Yellen B.B., Halverson D.S., Fridman G., Barbee K.A. & Friedman G. (2008) Validation of high gradient magnetic field based drug delivery to magnetizable implants under flow. *IEEE Trans Biomed Eng,* **55,** 643-9.

Friden P.M. (1994) Receptor-mediated transport of therapeutics across the blood-brain barrier. *Neurosurgery,* **35,** 294-8; discussion 298.

Friden P.M., Walus L.R., Musso G.F., Taylor M.A., Malfroy B. & Starzyk R.M. (1991) Anti-transferrin receptor antibody and antibody-drug conjugates cross the blood-brain barrier. *Proc Natl Acad Sci U S A,* **88,** 4771-5.

Gabathuler R. (2010) Approaches to transport therapeutic drugs across the blood-brain barrier to treat brain diseases. *Neurobiol Dis,* **37,** 48-57.

Gosk S., Vermehren C., Storm G. & Moos T. (2004) Targeting Anti-Transferrin Receptor Antibody (OX26) and OX26-Conjugated Liposomes to Brain Capillary Endothelial Cells Using In Situ Perfusion. *J Cereb Blood Flow Metab,* **24,** 1193-1204.

Green N.M. (1990) Avidin and streptavidin. *Methods Enzymol,* **184,** 51-67.

Herve F., Ghinea N. & Scherrmann J.M. (2008) CNS delivery via adsorptive transcytosis. *AAPS J,* **10,** 455-72.

Hong K., Zheng W., Baker A. & Papahadjopoulos D. (1997) Stabilization of cationic liposome-plasmid DNA complexes by polyamines and poly(ethylene glycol)-phospholipid conjugates for efficient in vivo gene delivery. *FEBS Letters,* **400,** 233-237.

Huwyler J., Wu D. & Pardridge W.M. (1996) Brain drug delivery of small molecules using immunoliposomes. *Proc Natl Acad Sci U S A,* **93,** 14164-9.

Huwyler J., Yang J. & Pardridge W.M. (1997) Receptor mediated delivery of daunomycin using immunoliposomes: pharmacokinetics and tissue distribution in the rat. *J Pharmacol Exp Ther,* **282,** 1541-6.

Iden D.L. & Allen T.M. (2001) In vitro and in vivo comparison of immunoliposomes made by conventional coupling techniques with those made by a new post-insertion approach. *Biochim Biophys Acta,* **1513,** 207-16.

Ishida T., Iden D.L. & Allen T.M. (1999) A combinatorial approach to producing sterically stabilized (Stealth) immunoliposomal drugs. *FEBS Lett,* **460,** 129-33.

Ivanov A.I. (2008) Pharmacological inhibition of endocytic pathways: is it specific enough to be useful? *Methods Mol Biol,* **440,** 15-33.

Jefferies W.A., Brandon M.R., Hunt S.V., Williams A.F., Gatter K.C. & Mason D.Y. (1984) Transferrin receptor on endothelium of brain capillaries. *Nature,* **312,** 162-3.

Jiang C., Koyabu N., Yonemitsu Y., Shimazoe T., Watanabe S., Naito M., Tsuruo T., Ohtani H. & Sawada Y. (2003) In vivo delivery of glial cell-derived neurotrophic factor across the blood-brain barrier by gene transfer into brain capillary endothelial cells. *Hum Gene Ther,* **14,** 1181-91.

Jiang C., Matsuo H., Koyabu N.*, et al.* (2002) Transluminal gene transfer into brain capillary endothelial cells in vivo with HVJ-liposomes. *J Drug Target,* **10,** 345-52.

Jing S.Q. & Trowbridge I.S. (1987) Identification of the intermolecular disulfide bonds of the human transferrin receptor and its lipid-attachment site. *EMBO J,* **6,** 327-31.

Kelley C., D'amore P., Hechtman H.B. & Shepro D. (1987) Microvascular pericyte contractility in vitro: comparison with other cells of the vascular wall. *The Journal of Cell Biology,* **104,** 483-490.

Kim J.A., Tran N.D., Li Z., Yang F., Zhou W. & Fisher M.J. (2005) Brain endothelial hemostasis regulation by pericytes. *J Cereb Blood Flow Metab,* **26,** 209-217.

Kolkova K., Novitskaya V., Pedersen N., Berezin V. & Bock E. (2000) Neural cell adhesion molecule-stimulated neurite outgrowth depends on activation of protein kinase C and the Ras-mitogen-activated protein kinase pathway. *J Neurosci,* **20,** 2238-46.

Kraal G. (1992) Cells in the marginal zone of the spleen. *Int Rev Cytol,* **132,** 31-74.

Kubo T., Sugita T., Shimose S., Nitta Y., Ikuta Y. & Murakami T. (2000) Targeted delivery of anticancer drugs with intravenously administered magnetic liposomes in osteosarcoma-bearing hamsters. *Int J Oncol,* **17,** 309-15.

Kurihara A. & Pardridge W.M. (1999) Imaging Brain Tumors by Targeting Peptide Radiopharmaceuticals through the Blood-Brain Barrier. *Cancer Research,* **59,** 6159-6163.

Leist M., Ghezzi P., Grasso G.*, et al.* (2004) Derivatives of erythropoietin that are tissue protective but not erythropoietic. *Science,* **305,** 239-42.

Li J.Y., Sugimura K., J.Boado R., Lee H.J., Zhang C., Duebel S. & M.Pardridge W. (1999) Genetically engineered brain drug delivery vectors: cloning, expression and in vivo application of an anti-transferrin receptor single chain antibody–streptavidin fusion gene and protein. *Protein Engineering,* **12,** 787-796.

Lichota J., Skjorringe T., Thomsen L.B. & Moos T. (2010) Macromolecular drug transport into the brain using targeted therapy. *J Neurochem,* **113,** 1-13.

Lin L.F., Doherty D.H., Lile J.D., Bektesh S. & Collins F. (1993) GDNF: a glial cell line-derived neurotrophic factor for midbrain dopaminergic neurons. *Science,* **260,** 1130-2.

Lowry O.H., Rosebrough N.J., Farr A.L. & Randall R.J. (1951) Protein measurement with the Folin phenol reagent. *J Biol Chem,* **193,** 265-75.

Lubbe A.S., Bergemann C., Huhnt W., Fricke T., Riess H., Brock J.W. & Huhn D. (1996a) Preclinical experiences with magnetic drug targeting: tolerance and efficacy. *Cancer Res,* **56,** 4694-701.

Lubbe A.S., Bergemann C., Riess H.*, et al.* (1996b) Clinical experiences with magnetic drug targeting: a phase I study with 4'-epidoxorubicin in 14 patients with advanced solid tumors. *Cancer Res,* **56,** 4686-93.

Löw H., Grebing C., Lindgren A., Tally M., Sun I.L. & Crane F.L. (1987) Involvement of transferrin in the reduction of iron by the transplasma membrane electron transport system. *Journal of Bioenergetics and Biomembranes,* **19,** 535-549.

Manjappa A.S., Chaudhari K.R., Venkataraju M.P., Dantuluri P., Nanda B., Sidda C., Sawant K.K. & Ramachandra Murthy R.S. (2011) Antibody derivatization and conjugation strategies: Application in preparation of stealth immunoliposome to target chemotherapeutics to tumor. *Journal of Controlled Release,* **150,** 2-22.

Martina M.-S., Fortin J.-P., Ménager C., Clément O., Barratt G., Grabielle-Madelmont C., Gazeau F., Cabuil V. & Lesieur S. (2005) Generation of Superparamagnetic Liposomes Revealed as Highly Efficient MRI Contrast Agents for in

Vivo Imaging. *Journal of the American Chemical Society,* **127,** 10676-10685.

Maruyama K., Takizawa T., Yuda T., Kennel S.J., Huang L. & Iwatsuru M. (1995) Targetability of novel immunoliposomes modified with amphipathic poly(ethylene glycol) s conjugated at their distal terminals to monoclonal antibodies. *Biochimica et Biophysica Acta (BBA) - Biomembranes,* **1234,** 74-80.

Mcbain S.C., Yiu H.H. & Dobson J. (2008) Magnetic nanoparticles for gene and drug delivery. *Int J Nanomedicine,* **3,** 169-80.

Moos T. (1996) Immunohistochemical localization of intraneuronal transferrin receptor immunoreactivity in the adult mouse central nervous system. *J Comp Neurol,* **375,** 675-92.

Moos T. (2002) Brain iron homeostasis. *Dan Med Bull,* **49,** 279-301.

Moos T. & Morgan E.H. (2001) Restricted transport of anti-transferrin receptor antibody (OX26) through the blood–brain barrier in the rat. *Journal of Neurochemistry,* **79,** 119-129.

Moos T. & Morgan E.H. (2002) A morphological study of the developmentally regulated transport of iron into the brain. *Dev Neurosci,* **24,** 99-105.

Moos T., Rosengren Nielsen T., Skjorringe T. & Morgan E.H. (2007) Iron trafficking inside the brain. *J Neurochem,* **103,** 1730-40.

Morgan E.H. & Moos T. (2002) Mechanism and developmental changes in iron transport across the blood-brain barrier. *Dev Neurosci,* **24,** 106-13.

Mount C. & Downton C. (2006) Alzheimer disease: progress or profit? *Nat Med,* **12,** 780-784.

Muldoon L.L., Pagel M.A., Kroll R.A., Roman-Goldstein S., Jones R.S. & Neuwelt E.A. (1999) A physiological barrier distal to the anatomic blood-brain barrier in a model of transvascular delivery. *AJNR Am J Neuroradiol,* **20,** 217-22.

Namdeo M., Saxena S., Tankhiwale R., Bajpai M., Mohan Y.M. & Bajpai S.K. (2008) Magnetic nanoparticles for drug delivery applications. *J Nanosci Nanotechnol,* **8,** 3247-71.

Nationalt Videnscenter for Demens N. (2011) Nyt diagnoseredskab hjælper læger med at stille Alzheimer-diagnosen. NVD, WEB: http://www.videnscenterfordemens.dk/forskning/forskningsnyheder/2011/12/nyt-diagnoseredskab-hjaelper-laeger-med-at-stille-alzheimer-diagnosen

Nationalt Videnscenter for Demens N. (2012) Alzheimers sygdom. WEB: http://www.videnscenterfordemens.dk/viden-om-demens/demenssygdomme/neurodegenerative-demenssygdomme/alzheimers-sygdom

Pardridge W.M. (1999) Vector-mediated drug delivery to the brain. *Advanced Drug Delivery Reviews,* **36,** 299-321.

Pardridge W.M. (2002) Drug and gene delivery to the brain: the vascular route. *Neuron,* **36,** 555-8.

Pardridge W.M. (2003) Blood-brain barrier drug targeting: the future of brain drug development. *Mol Interv,* **3,** 90-105, 51.

Pardridge W.M. (2005) The blood-brain barrier: bottleneck in brain drug development. *NeuroRx,* **2,** 3-14.

Pardridge W.M. (2010) Biopharmaceutical drug targeting to the brain. *Journal of Drug Targeting,* **18,** 157-167.

Pardridge W.M., Buciak J.L. & Friden P.M. (1991) Selective transport of an anti-transferrin receptor antibody through the blood-brain barrier in vivo. *J Pharmacol Exp Ther,* **259,** 66-70.

Pardridge W.M., Kang Y.-S. & Buciak J.L. (1994) Transport of Human Recombinant Brain-Derived Neurotrophic Factor (BDNF) Through the Rat Blood−Brain Barrier <i>in Vivo</i> Using Vector-Mediated Peptide Drug Delivery. *Pharmaceutical Research,* **11,** 738-746.

Paris-Robidas S., Emond V., Tremblay C., Soulet D. & Calon F. (2011) In vivo labeling of brain capillary endothelial cells after intravenous injection of monoclonal antibodies targeting the transferrin receptor. *Mol Pharmacol,* **80,** 32-9.

Penichet M.L., Kang Y.S., Pardridge W.M., Morrison S.L. & Shin S.U. (1999) An antibody-avidin fusion protein specific for the transferrin receptor serves as a delivery vehicle for effective brain targeting: initial applications in anti-HIV antisense drug delivery to the brain. *J Immunol,* **163,** 4421-6.

Peppiatt C.M., Howarth C., Mobbs P. & Attwell D. (2006) Bidirectional control of CNS capillary diameter by pericytes. *Nature,* **443,** 700-704.

Persidsky Y., Ramirez S.H., Haorah J. & Kanmogne G.D. (2006) Blood-brain barrier: structural components and function under physiologic and pathologic conditions. *J Neuroimmune Pharmacol,* **1,** 223-36.

Plateel M., Teissier E. & Cecchelli R. (1997) Hypoxia Dramatically Increases the Nonspecific Transport of Blood-Borne Proteins to the Brain. *Journal of Neurochemistry,* **68,** 874-877.

Qiao R., Jia Q., Hüwel S., Xia R., Liu T., Gao F., Galla H.-J. & Gao M. (2012) Receptor-Mediated Delivery of Magnetic Nanoparticles across the Blood–Brain Barrier. *ACS Nano,* **6,** 3304-3310.

Rivière C., Martina M.-S., Tomita Y., *et al.* (2007) Magnetic Targeting of Nanometric Magnetic Fluid–loaded Liposomes to Specific Brain Intravascular Areas: A Dynamic Imaging Study in Mice1. *Radiology,* **244,** 439-448.

Roberts R.L., Fine R.E. & Sandra A. (1993) Receptor-mediated endocytosis of transferrin at the blood-brain barrier. *J Cell Sci,* **104 (Pt 2),** 521-32.

Samad A., Sultana Y. & Aqil M. (2007) Liposomal drug delivery systems: an update review. *Curr Drug Deliv,* **4,** 297-305.

Sauer I., Dunay I.R., Weisgraber K., Bienert M. & Dathe M. (2005) An apolipoprotein E-derived peptide mediates uptake of sterically stabilized liposomes into brain capillary endothelial cells. *Biochemistry,* **44,** 2021-9.

Schneider C. & Williams J.G. (1985) Molecular dissection of the human transferrin receptor. *J Cell Sci Suppl,* **3,** 139-49.

Schnyder A. & Huwyler J. (2005) Drug transport to brain with targeted liposomes. *NeuroRx,* **2,** 99-107.

Seligman P.A. (1983) Structure and function of the transferrin receptor. *Prog Hematol,* **13,** 131-47.

Senyei A., Widder K. & G C. (1978) Magnetic Guidance of drug-carrying microspheres. *J. Appl. Phys., 49,* **49**.

Sharma A. & Sharma U.S. (1997) Liposomes in drug delivery: Progress and limitations. *International Journal of Pharmaceutics,* **154,** 123-140.

Shi N., Boado R.J. & Pardridge W.M. (2001) Receptor-mediated gene targeting to tissues in vivo following intravenous administration of pegylated immunoliposomes. *Pharm Res,* **18,** 1091-5.

Shi N. & Pardridge W.M. (2000) Noninvasive gene targeting to the brain. *Proc Natl Acad Sci U S A,* **97,** 7567-72.

Shigeoka A.A., Holscher T.D., King A.J., Hall F.W., Kiosses W.B., Tobias P.S., Mackman N. & Mckay D.B. (2007) TLR2 Is Constitutively Expressed within the Kidney and Participates in Ischemic Renal Injury through Both MyD88-Dependent and -Independent Pathways. *The Journal of Immunology,* **178,** 6252-6258.

Shin S.U., Wu D., Ramanathan R., Pardridge W.M. & Morrison S.L. (1997) Functional and pharmacokinetic properties of antibody-avidin fusion proteins. *J Immunol,* **158,** 4797-804.

Skaper S.D. (2008) The biology of neurotrophins, signalling pathways, and functional peptide mimetics of neurotrophins and their receptors. *CNS Neurol Disord Drug Targets,* **7,** 46-62.

Song B.W., Vinters H.V., Wu D. & Pardridge W.M. (2002) Enhanced neuroprotective effects of basic fibroblast growth factor in regional brain ischemia after conjugation to a blood-brain barrier delivery vector. *J Pharmacol Exp Ther,* **301,** 605-10.

Stojanov K., Georgieva J.V., Brinkhuis R.P., Van Hest J.C., Rutjes F.P., Dierckx R.A., De Vries E.F. & Zuhorn I.S. (2012) In vivo biodistribution of prion- and GM1-targeted polymersomes following intravenous administration in mice. *Mol Pharm*.

Strahan M.E., Crowe A. & Morgan E.H. (1992) Iron uptake in relation to transferrin degradation in brain and other tissues of rats. *Am J Physiol,* **263,** R924-9.

Tai L.M., Reddy P.S., Lopez-Ramirez M.A., Davies H.A., Male D.K., Loughlin A.J. & Romero I.A. (2009) Polarized P-glycoprotein expression by the immortalised human brain endothelial cell line, hCMEC/D3, restricts apical-to-basolateral permeability to rhodamine 123. *Brain Res,* **1292,** 14-24.

Triguero D., Buciak J. & Pardridge W.M. (1990) Capillary Depletion Method for Quantification of Blood–Brain Barrier Transport of Circulating Peptides and Plasma Proteins. *Journal of Neurochemistry,* **54,** 1882-1888.

Van Renswoude J., Bridges K.R., Harford J.B. & Klausner R.D. (1982) Receptor-mediated endocytosis of transferrin and the uptake of fe in K562 cells: identification of a nonlysosomal acidic compartment. *Proc Natl Acad Sci U S A,* **79,** 6186-90.

Wang J. & Pantopoulos K. (2011) Regulation of cellular iron metabolism. *Biochem J,* **434,** 365-81.

Wisse E., Braet F., Dianzhong Luo, De Zanger R., Jans D., Crabbe E. & Vermoesen A. (1996) Structure and Function of Sinusoidal Lining Cells in the Liver. *Toxicologic Pathology,* **24,** 100-111.

Witt K.A., Gillespie T.J., Huber J.D., Egleton R.D. & Davis T.P. (2001) Peptide drug modifications to enhance bioavailability and blood-brain barrier permeability. *Peptides,* **22,** 2329-2343.

Wolburg H. & Lippoldt A. (2002) Tight junctions of the blood-brain barrier: development, composition and regulation. *Vascul Pharmacol,* **38,** 323-37.

Wolburg H., Noell S., Mack A., Wolburg-Buchholz K. & Fallier-Becker P. (2009) Brain endothelial cells and the glio-vascular complex. *Cell Tissue Res,* **335,** 75-96.

Wolburg H., Wolburg-Buchholz K., Kraus J*., et al.* (2003) Localization of claudin-3 in tight junctions of the blood-brain barrier is selectively lost during experimental autoimmune encephalomyelitis and human glioblastoma multiforme. *Acta Neuropathol,* **105,** 586-92.

Wu D. & Pardridge W.M. (1999) Neuroprotection with noninvasive neurotrophin delivery to the brain. *Proc Natl Acad Sci U S A,* **96,** 254-9.

Wu D., Yang J. & Pardridge W.M. (1997) Drug targeting of a peptide radiopharmaceutical through the primate blood-brain barrier in vivo with a monoclonal antibody to the human insulin receptor. *The Journal of Clinical Investigation,* **100,** 1804-1812.

Yang H. (2010) Nanoparticle-mediated brain-specific drug delivery, imaging, and diagnosis. *Pharm Res,* **27,** 1759-71.

Zak O., Trinder D. & Aisen P. (1994) Primary receptor-recognition site of human transferrin is in the C-terminal lobe. *J Biol Chem,* **269,** 7110-4.

Zhang Y.-F., Wang J.-C., Bian D.-Y., Zhang X. & Zhang Q. (2010) Targeted delivery of RGD-modified liposomes encapsulating both combretastatin A-4 and doxorubicin for tumor therapy: In vitro and in vivo studies. *European Journal of Pharmaceutics and Biopharmaceutics,* **74,** 467-473.

Zhang Y., Boado R.J. & Pardridge W.M. (2003a) In vivo knockdown of gene expression in brain cancer with intravenous RNAi in adult rats. *The Journal of Gene Medicine,* **5,** 1039-1045.

Zhang Y., Calon F., Zhu C., Boado R.J. & Pardridge W.M. (2003b) Intravenous nonviral gene therapy causes normalization of striatal tyrosine hydroxylase and reversal of motor impairment in experimental parkinsonism. *Hum Gene Ther,* **14,** 1-12.

Zhang Y., Schlachetzki F., Zhang Y.F., Boado R.J. & Pardridge W.M. (2004) Normalization of striatal tyrosine hydroxylase and reversal of motor impairment in experimental parkinsonism with intravenous nonviral gene therapy and a brain-specific promoter. *Hum Gene Ther,* **15,** 339-50.

Zhang Y.F., Boado R.J. & Pardridge W.M. (2003c) Absence of toxicity of chronic weekly intravenous gene therapy with pegylated immunoliposomes. *Pharm Res,* **20,** 1779-85.

Zlokovic B.V. (2008) The blood-brain barrier in health and chronic neurodegenerative disorders. *Neuron,* **57,** 178-201.

7. Appendix

7.1 Calculating the antibody density per OX26-ML

$Numbers\ used\ for\ the\ calculation;$

$Mass\ of\ OX26 - MLs/mL\ 0.0013\ g$

$Molecular\ weight\ of\ OX26 = 160{,}000\ g/mol$

$Mass\ of\ OX26/mL = 0.00054\ \mathrm{g}$

$Predicted\ particles\ number\ from\ the\ manufactorer = 1.8 \times 10^{15} particles/\ g$

$Amount\ of\ OX26\ pr.mL\ in\ mol$

$$n = \frac{m}{M} = \frac{0.00054\ g}{160{,}000\ g/mol} = 3.37 \times 10^{-09}\ mol$$

$Converting\ to\ number\ of\ OX26\ antibodies$

$3.37 \times 10^{-09}\ mol \times 6.02214 \times 10^{23} = 2.03 \times 10^{15}$

$Calculating\ the\ number\ of\ particles\ pr.mL, assuming\ there\ is\ 1.8 \times 10^{15} particles/\ g$

$0.0013\ g \times 1.8 \times 10^{15} = 2.34 \times 10^{12}$

$Calculating\ the\ OX26\ density$

$$Antibody\ density = \frac{2.03 \times 10^{15}}{2.34 \times 10^{12}} = 868$$